International Journal of
STEEL STRUCTURES

Ultimate Behavior of Steel Cable-stayed Bridges - I. Rational Ultimate Analysis Method -

Seungjun Kim[1], Deok Hee Won[2], and Young Jong Kang[3,*]

[1]*Assistant Professor, Department of Construction Safety and Disaster Prevention Engineering, Daejeon University, Daejeon, Korea*
[2]*Senior Research Scientist, Coastal Development & Ocean Energy Research Division, Korea Institute of Ocean Science and Technology, Ansan, Korea*
[3]*Professor, School of Architectural, Civil and Environmental Engineering, Korea University, Seoul, Korea*

Abstract

This paper presents an investigation on the ultimate behavior of steel cable-stayed bridges. In general, various nonlinear factors affect the global behavior of cable-stayed bridges, such as material nonlinearities, cable-sag effect, beam-column effect, large displacement effect, and girder-mast-cable interaction. These effects also affect the ultimate behavior of cable-stayed bridges. Therefore, a rational analysis method should be performed to study the ultimate behavior of cable-stayed bridges. Because of various nonlinearities, the analysis should be based on the theory of nonlinear finite element analysis. Moreover, rational ultimate analysis can reflect characteristics of the design and construction of cable-stayed bridges. In this study, a rational ultimate analysis method for steel cable-stayed bridges is developed and proposed based on the theory of nonlinear finite element analysis. A two-step analysis method is proposed and used in this study. Through this analysis scheme, the structural state under dead load is considered before the live load analysis. The developed program is used to study the ultimate behavior of steel cable-stayed bridges under vertically applied live load cases. Analytical study is used to investigate governing ultimate modes under the considered live load cases. By comparing the analysis results under each live load case, the critical load case is determined. The effects of geometric nonlinearities and material nonlinearities on the ultimate behavior of steel cable-stayed bridges are studied by performing geometric nonlinear analysis, as well as ultimate analysis.

Keywords: cable-stayed bridges, nonlinear analysis, initial shape analysis, refined plastic hinge method, generalized displacement control method

1. Introduction

Because of the excellent structural efficiency, cable-stayed bridges have been mainly constructed for long-span bridges. Bridge systems generally have many columns or piers to support the superstructure. In contrast, cable-stayed bridges are supported by stay cables, which are designed as the intermediate support members of the girder. Vertical components of the tensile forces of cables hang on the girder. Thus, cable-stayed structures are suitable for long-span bridges.

The cable-stayed bridge is a composite system of girder, mast, and cables. Each main member shows a different structural behavior. The girder is basically designed as a flexural member, while the mast and cable is designed as a compression member and tensile member, respectively. When external forces are applied to the girder, these forces are finally transferred to ground via the cables and masts, because the girder, mast and cables are connected to each other. Because of the composition of the main members that show different structural behavior, cable-stayed bridges exhibit extreme structural efficiency and performance.

As is well known, cable-stayed bridges show complex structural behavior, because of various nonlinearities (Adeli and Zhang, 1994; Xi and Kuang, 1999; Ren, 1999; Freire *et al.*, 2006). The following factors lead to the nonlinear behavior of cable-stayed bridges: the first is the cable-sag effect initiated by its own weight; and the second is the beam-column effect of the girder and mast, which is induced by their flexural behavior under applied compressive forces. Also, the large displacement or deformation effect produced by the geometric change of the structure leads to geometric nonlinear behavior.

Furthermore, the girder-mast-cable interaction affects the complex nonlinear behavior. When external load is applied to the girder first, it is transferred to the mast by stayed cables, which connect the girder and mast. Because of the connection between the main members, the local structural behavior of each member affects the behavior of other members, which may result in global behavior and global changes of structural state.

Because of various geometric nonlinearities mentioned previously with material nonlinearities, the ultimate behavior of cable-stayed bridges can also be induced by various causes, such as material yield, elastic/inelastic buckling of the girder and/or mast, fatigue, and local failure. Therefore, a rational ultimate analysis method should be performed to investigate the ultimate behavior of cable-stayed bridges. For the rational analysis, nonlinear analysis can be adopted because it can consider the various nonlinearities of cable-stayed bridges. Moreover, nonlinear analysis performed by the iterative-incremental analysis can also reflect the structural change (such as stiffness change, material yield or buckling of some member or element) as the external loads change. Therefore, the ultimate analysis of cable-stayed bridges should be considered based on nonlinear analysis.

Studies to investigate the structural stability or ultimate behavior of cable-stayed bridges have been performed by several researchers. This research has been performed to investigate the structural stability of completed cable-stayed bridges using eigenvalue analysis (Tang *et al.*, 2001; Shu and Wang, 2001). Various elastic buckling modes were introduced, and the effects of various geometric properties on the structural stability were described. But various nonlinearity factors were not considered,, because these studies were conducted by conventional eigenvalue analysis. Furthermore, the initial condition, which can be considered by initial shape analysis, was not considered before considering the live load condition. This is very important, because cable-stayed bridges are designed with proper initial tensile forces of cables, which make for minimum deformation and internal forces under dead load condition (Chen *et al.*, 2000; Cheng and Xiao, 2007; Kim and Lee, 2001; Wang *et al.*, 1993; Wang and Yang, 1993).

Studies to investigate the ultimate behavior have been performed using nonlinear analysis by several researchers. The ultimate behavior and capacity of concrete cable-stayed bridges were investigated by Ren (1999), who considered various nonlinearities, boundary condition and loading conditions. But in that study also, initial shape analysis to consider the structural state under the dead load condition was not performed before the live load analysis. Moreover, detailed structural behavior as the external load changes is not described. A nonlinear analysis method for obtaining the ultimate capacity of cable-stayed bridges was suggested by Song and Kim (2007), who considered geometric and material nonlinearities. They suggested a type of two-step

analysis, which consists of initial shape analysis and live load analysis. In this analysis method, the beam-column element and conventional equivalent truss element were used to model the girder, mast, and cable. For the incremental-iterative numerical solution, the Newton-Rapshon method was used, which cannot trace the complex nonlinear problem. In addition, a relatively simple analytical model was used to investigate the ultimate behavior of cable-stayed bridges, and the procedure of ultimate behavior wasn't described in detail.

For investigation of the ultimate behavior of cable-stayed bridges, nonlinear analysis should basically be performed to consider various nonlinearities. Also, the structural state under the dead load condition should be considered before live load analysis, because of the characteristics of the design and construction of cable-stayed bridges. Thus, ultimate analysis for investigation of the ultimate behavior under various live load conditions should be performed by a multi-analysis step. In addition, suitable finite elements should be used to model the girder, mast and cables; and a suitable numerical scheme for the incremental-iterative analysis should be adopted to trace the complex nonlinear response and ultimate behavior.

In this study, the ultimate behavior of steel cable-stayed bridges is investigated and presented. A rational ultimate analysis method based on the theory of nonlinear analysis is first proposed. For modeling the girder, mast and cable, a nonlinear frame element and nonlinear equivalent truss element are used. For considering the material nonlinearity of steel members, the refined plastic hinge method is adopted. In addition, the generalized displacement control method is used for the incremental-iterative analysis scheme. The proposed analysis method is performed as a two-step analysis, which consists of initial shape analysis and live load analysis. Using the proposed method, the ultimate behavior of long-span steel cable-stayed bridges under specific live load cases is described in detail, with various quantitative data such as load-displacement curves, load-cable force curves, deformations, and moment diagram change. Through the detailed observation of analysis results, the governing factors which cause the ultimate behavior of steel cable-stayed bridges are studied and described.

2. Theoretical Background

Ultimate analysis of steel cable-stayed bridges should be performed by considering various nonlinearities. In this chapter, the theoretical background is introduced. Firstly, geometric nonlinear elements for modeling the main members of cable-stayed bridges are described, and the method for considering the material nonlinearity of steel members is introduced. Secondly, a numerical strategy for incremental-iterative analysis is described. Finally, an analysis scheme for a two-step ultimate analysis of steel cable-stayed bridges is proposed.
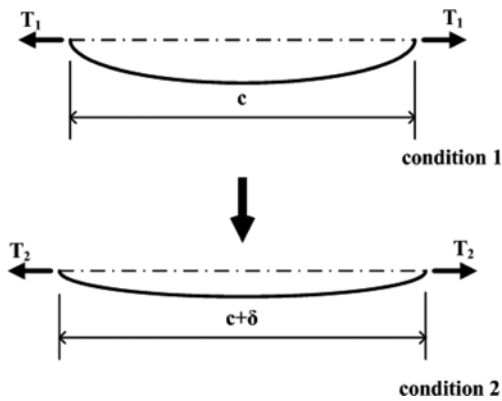
Figure 1. Two conditions for a horizontal stay cable with tensile forces T_1 and T_2, respectively.
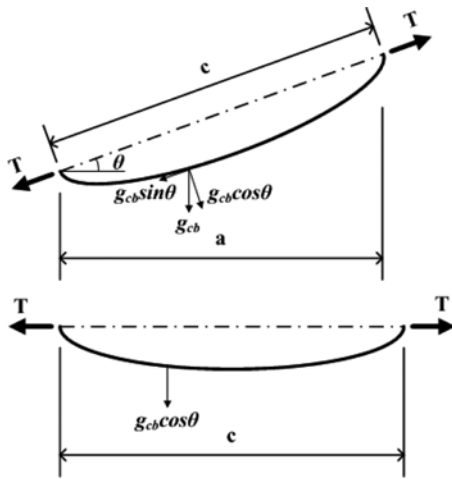

Figure 2. Inclined stay cable and equivalent horizontal stay cable with equal deformational characteristics (g_{cb}: weight per unit length of a cable, T: tensile force).

2.1. Cable element

In this study, a nonlinear equivalent truss element was adopted as the cable element. The equivalent truss element is a modified truss element, which uses an equivalent elastic modulus in order to consider the sag effect of the cable. The following figures show the configurations of horizontal and inclined stay cables.

This element has 2 nodes and 3 degrees of freedom. As shown in Eq. (1), the stiffness matrix of the equivalent truss element has an equivalent elastic modulus, which considers the cable-sag effect defined by the weight and tensile force of a cable member. In other words, the tangential or secant modulus calculated by the equation for considering the cable-sag effect replaces the elastic modulus in the stiffness matrix of the truss element (Ernst, 1965; Flemning, 1979; Gimsing, 1983). Therefore, the stiffness matrix can be written by using the tangential or secant elastic modulus as follows:

$$[k] = [k_e] + [k_g] = \frac{{}^1E_{eq} + {}^1A}{{}^1L} \begin{bmatrix} 1 & 0 & 0 & -1 & 0 & 0 \\ & 0 & 0 & 0 & 0 & 0 \\ & & 0 & 0 & 0 & 0 \\ & & & 1 & 0 & 0 \\ & & & & 0 & 0 \\ & & & & & 0 \end{bmatrix}$$

$$+ \frac{{}^1\tau_{11} + {}^1A}{{}^1L} \begin{bmatrix} 1 & 0 & 0 & -1 & 0 & 0 \\ & 1 & 0 & 0 & -1 & 0 \\ & & 1 & 0 & 0 & -1 \\ & & & 1 & 0 & 0 \\ & & & & 1 & 0 \\ & & & & & 1 \end{bmatrix} \quad (1)$$

where

$[k]$ = stiffness matrix of a nonlinear equivalent truss element

$[k_e]$ = elastic stiffness matrix

$[k_g]$ = geometric stiffness matrix

${}^1E_{eq}$ = ${}^1E_{tan}$ or ${}^1E_{sec}$

${}^1E_{tan}$ = tangential modulus

${}^1E_{sec}$ = secant modulus

${}^1\tau_{11}$ = axial stress of a cable member

${}^1A$ = sectional area of a cable member

${}^1L$ = length of a cable members

(Left superscript refers to the occurring configurations as below: 0: initial undeformed configuration, 1: last calculated configuration, 2: current deformed configuration)

Incidentally, the previous equations for the tangential and secant elastic modulus of the cable were derived by using the equation of elastic catenary shape function, simplified by Taylor's series. For example, the hyperbolic *sine* (x) and *cosine* (x) terms in that shape function were substituted for by $(x+x^3/6)$ and *1*, respectively (Ernst, 1965; Flemming, 1979; Gimsing, 1983; Freire *et al.*, 2006; Xi and Kuang, 1999; Ren, 1999; Adeli and Zhang, 1994; Wang and Yang, 1993; Wang *et al.*, 1993; Wang *et al.*, 2002). If a sufficiently large tensile force is applied to the cable member, a large numerical error might not occur, although the stiffness matrix with this equivalent modulus is used for the structural analysis. However, if a small tensile force is applied to the cable member, the stiffness matrix using this equivalent modulus might cause a large numerical error, because of this simplification.

In this study, the equivalent elastic modulus, which is derived without any simplification of shape function of the elastic catenary, is used for the stiffness matrix of the cable member. The equation for the equivalent elastic modulus is as follows: (Kim *et al.*, 2006; Kim, 2010)

$$E_{\tan} = \frac{E}{(1+K_1+K_2)/2\cosh\left(\frac{g_{cb}a}{2T_i}\right)} \tag{2}$$

where

$$K_1 = \frac{1}{g_{cb}a}\left[2T_i\sinh\left(\frac{g_{cb}a}{T_i}\right) - g_{cb}a \cdot \sinh\left(\frac{g_{cb}a}{T_i}\right)\right]$$

$$K_2 = \frac{-4EA}{g_{cb}a}\left[\sinh\left(\frac{g_{cb}a}{2T_i}\right) - \frac{g_{cb}a}{2T_i} \cdot \cosh\left(\frac{g_{cb}a}{2T_i}\right)\right]$$

$$E_{\sec} = \frac{(T_f - T_i)}{\frac{\delta}{c}} = \frac{E}{(1+K_1+K_2)/2\cosh\left(\frac{g_{cb}a}{2T_f}\right)} \tag{3}$$

where

$$K_1 = \frac{1}{g_{cb}a(T_f - T_i)}\left[T_f^2\sinh\left(\frac{g_{cb}a}{T_f}\right) - T_i^2\sinh\left(\frac{g_{cb}a}{T_i}\right)\right]$$

$$K_2 = \frac{4EA}{g_{cb}a(T_f - T_i)}\left[T_i\sinh\left(\frac{g_{cb}a}{2T_i}\right) - T_f\sinh\left(\frac{g_{cb}a}{2T_f}\right)\right]$$

g_{cb} = weight per unit length of the cable
T_i = tensile force at condition 1
T_f = tensile force at condition 2
a = horizontally projected length of the cable

As shown by the above equations, there are two equivalent moduli. The first one is the tangential modulus, and the other one is the secant modulus. When the secant modulus is used for the equivalent modulus, the resultant force at Condition 2 should be considered. The resultant force of the cable element is unknown in every incremental-iterative analysis. Therefore, additional analyses are needed to determine the secant modulus of cable members. In contrast, when the tangential modulus of the cable member is used, no additional analyses are needed to determine the equivalent modulus. In every incremental-iterative analysis, only the tensile force at Condition 1 (that is, the current condition before incremental forces are applied) is used to calculate the equivalent modulus. Because the proposed analysis method is based on nonlinear analysis with incremental-iterative solution strategy, the tangential modulus is more suitable for an equivalent modulus than the secant modulus. Thus, the tangential modulus is adopted as the equivalent modulus of the nonlinear equivalent truss element.

2.2. Nonlinear frame element

Because the girder and mast of cable-stayed bridges are subjected to compressive force while bending behavior occurs, nonlinear frame elements derived by an updated Lagrangian formulation are used for modeling the girder and mast. Figure 4 presents the nodal displacements and forces of the nonlinear frame element used in this study. As shown in this figure, there are six displacement components and six force components at one node. In the derived procedure of the stiffness matrix, the high order
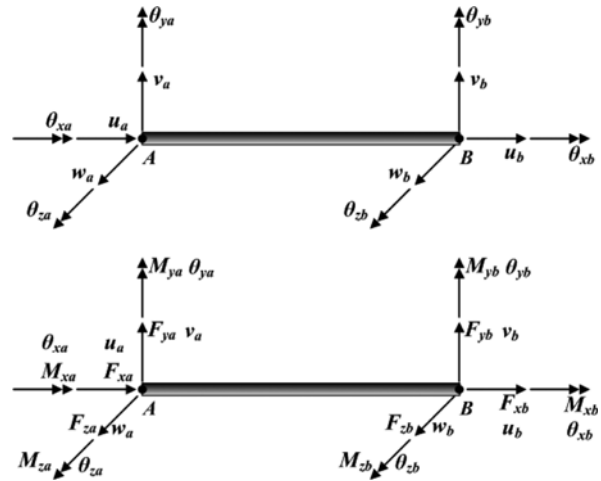

Figure 4. Nodal displacements and forces of the nonlinear frame element.

terms of the strain are considered, and the additional induced stiffness matrix is adopted, as well as the elastic and geometric stiffness matrix of the nonlinear frame element (Yang and Kuo, 1993; Lim *et al.*, 2008; Kim, 2010).

The following equation describes the stiffness matrix, composed of elastic, geometric and induced stiffness matrices.

$$[k] = [k_e] + [k_g] + [k_i] \tag{4}$$

where
$[k_e]$ = elastic stiffness matrix
$[k_g]$ = geometric stiffness matrix
$[k_i]$ = induced stiffness matrix

$$[k_g] = \begin{bmatrix} a & 0 & 0 & 0 & -d & -e & -a & 0 & 0 & 0 & -n & -o \\ & b & 0 & d & g & k & 0 & -b & 0 & n & -g & k \\ & & c & e & -h & g & 0 & 0 & -c & o & -h & -g \\ & & & f & i & l & 0 & -d & -e & -f & -i & -l \\ & & & & j & 0 & d & -g & h & -i & p & -q \\ & & & & & m & e & -k & -g & -l & q & r \\ & & & & & & a & 0 & 0 & 0 & n & o \\ & & & & & & & b & 0 & -n & g & -k \\ & & & & & & & & c & -o & h & g \\ & & & & & & & & & f & i & l \\ & & & & & & & & & & j & 0 \\ & & & & & & & & & & & m \end{bmatrix} \tag{5}$$

where

$$a = \frac{{}^1F_{xb}}{{}^1L}, \quad b = \frac{6\,{}^1F_{xb}}{5\,{}^1L} + \frac{12\,{}^1F_{xb}I_z}{A\,{}^1L^3}, \quad c = \frac{6\,{}^1F_{xb}}{{}^1L} + \frac{12\,{}^1F_{xb}I_y}{A\,{}^1L^3},$$

$$d = \frac{{}^1M_{ya}}{{}^1L}, \quad e = \frac{{}^1M_{za}}{{}^1L}, \quad f = \frac{{}^1F_{xb}J}{A\,{}^1L}, \quad g = \frac{{}^1M_{xb}}{{}^1L},$$

$$h = \frac{^1F_{xb}}{10} + \frac{6\,^1F_{xb}I_y}{A^1L^2}, \quad i = \frac{^1M_{za} + ^1M_{zb}}{6},$$

$$j = \frac{2\,^1F_{xb}\,^1L}{15} + \frac{4\,^1F_{xb}I_y}{A^1L}, \quad k = \frac{^1F_{xb}}{10} + \frac{6\,^1F_{xb}I_z}{A^1L^2},$$

$$l = -\frac{^1M_{ya} + ^1M_{yb}}{6}, \quad m = \frac{2\,^1F_{xb}\,^1L}{15} + \frac{4\,^1F_{xb}I_z}{A^1L}, \quad n = \frac{^1M_{yb}}{^1L}$$

$$o = \frac{^1M_{zb}}{^1L}, \quad p = \frac{^1F_{xb}\,^1L}{30} + \frac{2\,^1F_{xb}I_y}{A^1L}, \quad q = -\frac{^1M_{xb}}{2},$$

$$r = \frac{^1F_{xb}\,^1L}{30} + \frac{2\,^1F_{xb}I_z}{A^1L}$$

A = sectional area of the frame element
L = length of the frame element
I_y, I_z = 2nd moment of inertia with respect to the y and
       z axis, respectively
J = torsional constant

$$[k_i] = \begin{bmatrix} [0] & & & \\ & [k_i]_a & & \\ & & [0] & \\ & & & [k_i]_b \end{bmatrix} \qquad (6)$$

where

$$[k_i]_a = \begin{bmatrix} 0 & 0 & 0 \\ ^1M_{za} & 0 & -^1M_{xa}/2 \\ -^1M_{ya}/2 & ^1M_{xa}/2 & 0 \end{bmatrix}$$

$$[k_i]_b = \begin{bmatrix} 0 & 0 & 0 \\ ^1M_{zb} & 0 & -^1M_{xb}/2 \\ -^1M_{yb}/2 & ^1M_{xb}/2 & 0 \end{bmatrix}$$

2.3. Refined plastic hinge method

There are several methods for considering material nonlinearities in nonlinear analysis using a beam or frame element. These are plastic zone analysis, plastic hinge analysis and refined plastic hinge analysis, as shown in Fig. 3.

Using the plastic zone method, the member is divided along its axial axis into sections of finite elements; each sectional members, is also further divided into several elements, as shown in Fig. 3. Stresses are calculated to consider the material nonlinearity for each element in a section of a member. So, the most accurate analysis results may be obtained when the plastic zone method is used as the method to consider material nonlinearity; but unfortunately the most calculation time is also required. When the plastic hinge method is used as the method to consider material nonlinearity, the tangential modulus is used instead of the elastic modulus for considering the gradual yield of the materials. Using this method, additional elemental division of the section is not required. So, the calculation time can be reduced when compared with the plastic zone method; but unfortunately this method can only consider a gradual yield induced by the axial force. In other words, the gradual yield induced by other member forces cannot be considered. For example, the girder and mast of a cable-stayed bridge are subjected to bending moment as well as to axial force. So, the plastic hinge method is not suitable for the material nonlinear analysis
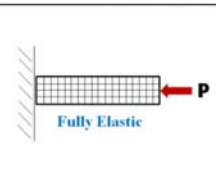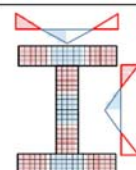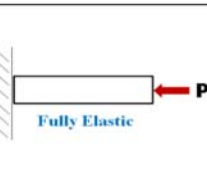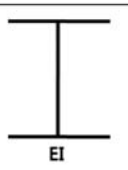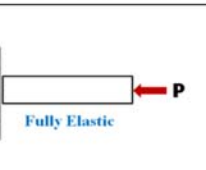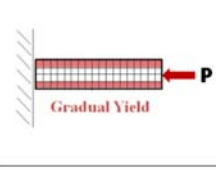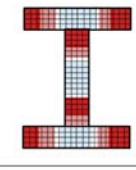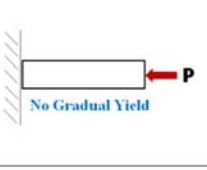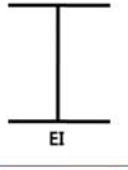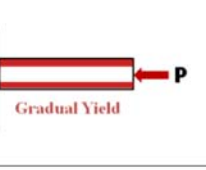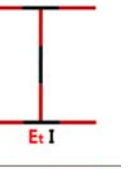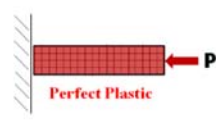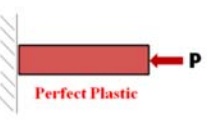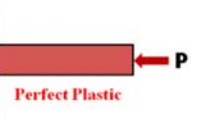

Figure 3. Analysis methods for considering material nonlinearities.

of steel cable-stayed bridges, despite the advantage of having the smallest required calculation time. Therefore, for accurate and efficient material nonlinear analysis using beam or frame elements, the refined plastic hinge method was developed (Liew *et al.*, 1993). Using this method, the effect of a gradual yield by the forces of a main member of the beam/frame element can be efficiently considered. In order to consider the effect of the axial and bending moment, a tangential modulus and plastic hinge parameter are introduced into the elastic matrix of the frame elements. The following equations show the tangential modulus for steel members:

$$E_t = E \quad \text{for} \quad P < 0.5P_y \tag{7}$$

$$E_t = 4\frac{P}{P_y}\left(1 - \frac{P}{P_y}\right)E \quad \text{for} \quad P > 0.5P_y \tag{8}$$

In general, the steel members have residual stresses, so gradual yield occurs when axial force is applied to the section of the member. For considering the effect of the gradual yield induced by axial force, the Column Research Council (CRC) tangential equation (Galambos, 1988) was employed to derive the tangent modulus, considering 50.0% of the yield stress of a member as the maximum compressive residual stress. In fact, it is possible for the equation correction to consider $\alpha\%$ of the yield stress as the maximum residual stress. But, in this study, the maximum residual stress assumes 50.0% of the yield stress as the

maximum residual stress. So, the conventional tangential modulus presented by the refined plastic hinge method is adopted to consider the effect of gradual yield by axial forces.

An advantage of the refined plastic hinge method is that it can consider the gradual yield by bending moment. In other to consider this effect, the scalar parameter η is employed for the elastic stiffness of the beam/frame elements.

$$\eta = 1.0 \quad \text{for} \quad \alpha < 0.5 \tag{9}$$

$$\eta = 4\alpha(1 - \alpha) \quad \text{for} \quad \alpha < 0.5 \tag{10}$$

where η is the scalar parameter, and the term α is expressed as

$$\alpha = \frac{P}{P_y} + \frac{8}{9}\frac{M_y}{M_{yp}} + \frac{8}{9}\frac{M_z}{M_{zp}} \quad \text{for} \quad \frac{P}{P_y} \geq \frac{2}{9}\frac{M_y}{M_{yp}} + \frac{2}{9}\frac{M_z}{M_{zp}} \tag{11}$$

$$\alpha = \frac{P}{2P_y} + \frac{M_y}{M_{yp}} + \frac{M_z}{M_{zp}} \quad \text{for} \quad \frac{P}{P_y} < \frac{2}{9}\frac{M_y}{M_{yp}} + \frac{2}{9}\frac{M_z}{M_{zp}} \tag{12}$$

where α expresses the level of internal forces of the frame element based on the equation of the beam-column member design in the AISC-LRFD specification (1994)

Based on the tangential modulus and scalar parameter η, the elastic stiffness matrix of the nonlinear frame element is rewritten as follows to consider the effect of gradual yield induced by axial force and bending moment:

Bending in the $\hat{x} - \hat{y}$ plane,

$$[k] = \frac{EI_z}{L} \times \begin{bmatrix} v_a & \theta_{za} & v_b & \theta_{zb} \\ \dfrac{3\eta_A + 6\eta_A\eta_B + 3\eta_B}{L^2} & \dfrac{3\eta_A + 3\eta_A\eta_B}{L} & -\dfrac{3\eta_A + 6\eta_A\eta_B + 3\eta_B}{L^2} & \dfrac{3\eta_B + 3\eta_A\eta_B}{L} \\ \dfrac{3\eta_A + 3\eta_A\eta_B}{L} & 3\eta_A + \eta_A\eta_B & -\dfrac{3\eta_A + 3\eta_A\eta_B}{L} & 2\eta_A\eta_B \\ -\dfrac{3\eta_A + 6\eta_A\eta_B + 3\eta_B}{L^2} & -\dfrac{3\eta_A + 3\eta_A\eta_B}{L} & \dfrac{3\eta_A + 6\eta_A\eta_B + 3\eta_B}{L^2} & -\dfrac{3\eta_B + 3\eta_A\eta_B}{L} \\ \dfrac{3\eta_B + 3\eta_A\eta_B}{L} & 2\eta_A\eta_B & -\dfrac{3\eta_B + 3\eta_A\eta_B}{L} & 3\eta_B + \eta_A\eta_B \end{bmatrix} \tag{13}$$

Bending in the $\hat{x} - \hat{z}$ plane,

$$[k] = \frac{EI_z}{L} \times \begin{bmatrix} w_a & \theta_{ya} & w_b & \theta_{yb} \\ \dfrac{3\eta_A + 6\eta_A\eta_B + 3\eta_B}{L^2} & -\dfrac{3\eta_A + 3\eta_A\eta_B}{L} & -\dfrac{3\eta_A + 6\eta_A\eta_B + 3\eta_B}{L^2} & -\dfrac{3\eta_B + 3\eta_A\eta_B}{L} \\ -\dfrac{3\eta_A + 3\eta_A\eta_B}{L} & 3\eta_A + \eta_A\eta_B & \dfrac{3\eta_A + 3\eta_A\eta_B}{L} & 2\eta_A\eta_B \\ -\dfrac{3\eta_A + 6\eta_A\eta_B + 3\eta_B}{L^2} & \dfrac{3\eta_A + 3\eta_A\eta_B}{L} & \dfrac{3\eta_A + 6\eta_A\eta_B + 3\eta_B}{L^2} & -\dfrac{3\eta_B + 3\eta_A\eta_B}{L} \\ -\dfrac{3\eta_B + 3\eta_A\eta_B}{L} & 2\eta_A\eta_B & \dfrac{3\eta_B + 3\eta_A\eta_B}{L} & 3\eta_B + \eta_A\eta_B \end{bmatrix} \tag{14}$$

It should be noted that:
(1) When $1 > \eta_A > 0$ and $1 > \eta_B > 0$, these account for the effects of partial yield at both ends of the elements.
(2) When $\eta_i = 1$, the section of node i is fully elastic.
(3) When $0 < \eta_i < 1$, the section of the node i is partially yielding.
(4) When $\eta_i = 0$, the section of node i has fully yielded.

2.4. Incremental-iterative analysis scheme

In order to trace the nonlinear response, a rational and effective incremental-iterative solving strategy should be considered. Such analysis schemes can be classified into several categories, including the force-control method, displacement-control method, and work control method. In general, the Newton-Rapshon method, a type of force-control method, is widely used for the numerical scheme of the nonlinear problem. However, this method is not suitable for nonlinear analysis of a structure that shows complex nonlinear behavior and structurally unstable states, because changeable load factors cannot be considered.

In many cases of complex nonlinear problems, the numerical scheme based on the displacement-control method or work-control method is widely adopted, and the arc-length method is one of the most used methods for nonlinear problems. Using this method, the incremental-iterative load factor is determined based on the following constraint equation, considering the structural state at each incremental-iterative analysis step (Crisfield, 1983).

$$\{\Delta U_1\}^T \{\Delta U_j\} + \lambda_1 \lambda_j = \Delta S^2 \qquad (15)$$

where,
$\{\Delta U_1\}$ = displacement increments for the first iteration
$\{\Delta U_j\}$ = displacement increments for the j-th iteration
λ_1 = incremental-iterative load factor for the first iteration
λ_j = incremental-iterative load factor for the j-th iteration
ΔS = arc length

However, there is the logical problem of the inequality of the units of each term. As shown in the Constraint Eq. (15), the units of the first term on the left side and the term on the right side are a square length, while the second term on the left side is a non-dimensional constant. Therefore, another numerical scheme, other than the arc-length method, should be adopted for solving complex nonlinear problems.

In this study, the generalized displacement control method (Yang and Kuo, 1993; Lim et al., 2008; Kim, 2010) is adopted. The following equations are used for the determination of the incremental-iterative load factor at each analysis step:

$$\lambda_1 = \pm \lambda_1^1 |GSP|^{1/2} \quad (j=1) \qquad (16)$$

$$\lambda_j = -\frac{\{\Delta \hat{U}_1^{i-1}\}^T \{\Delta \overline{U}_j\}}{\{\Delta \hat{U}_1^{i-1}\}^T \{\Delta \hat{U}_j\}} \quad (j \geq 2) \qquad (17)$$

where

$$GSP = \frac{\{\Delta \hat{U}_1^1\}^T \{\Delta \hat{U}_1^1\}}{\{\Delta \hat{U}_1^{i-1}\}^T \{\Delta \hat{U}_1\}}, \text{ Generalized stiffness parameter}$$

λ_j = i-th incremental, j-th iterative analysis load factor
λ_1^1 = preset load increment factor
$\{\Delta \overline{U}\}$ = incremental displacement vector by unbalanced force vector
$\{\Delta \hat{U}\}$ = incremental displacement vector by total load vector

(A super script indicates an incremental step while a subscript indicates an iterative step. All quantities with no superscript should be interpreted as those associated with the i-th incremental step.)

The sign of λ_1^1 at the right side in Eq. (16) indicates the load applying direction. If the sign is positive, the incremental load is applied in the same direction as that of the former incremental load. This sign is determined by the sign of GSP, the generalized stiffness parameter described in Equation (17). If GSP has a positive sign, the sign of λ_1 has the same sign as that of λ_1^{i-1}, which refers to the former incremental load factor. However, if GSP shows a negative sign, the direction of loading is reversed by multiplying the λ_1 by −1.

2.5. Nonlinear analysis procedure

Based on the incremental-iterative analysis scheme introduced in previous section, the nonlinear finite element analysis is performed calculating all the displacements and internal forces at every nodes of the analysis model. First of all, the applied external force vector $\{P_j^i\}$ at j-th iteration of the i-th incremental analysis step can be written as shown in Eq. (18).

$$\{P_j^i\} = \Lambda_j^i \{\hat{P}\} \qquad (18)$$

where, $\{\hat{P}\}$ is the reference load vector which denotes the total applied load vector, $\Lambda_j^i = \Lambda_{j-1}^i + \lambda_j^i$ is the load increment parameter at j-th iteration of the i-th incremental analysis step, λ_j^i = load factor shown in Eqs (16) and (17)

The incremental-iterative analysis is conducted as follows:
Step 1: Calculate the displacement increments $\{\Delta U_j^i\}$ and load increment parameter λ_j^i
A. For the first iteration (j =1) at any incremental step i
(a) Set the global structural stiffness matrix $[K_0^i]$
(b) Solve the following equation for calculating the displacement vector $\{\Delta \hat{U}_1\}$ due to reference load vector $\{P\}$ at the current state

$$[K_{j-1}^i]\{\Delta\hat{U}_1^j\} = \{\hat{P}\} \qquad (19)$$

(c) If $i=1$, set GSP as 1.0

If $i>1$, use Eq. (12) to calculate GSP and λ_1^i

(d) If the calculated GSP is negative, multiply the λ_1^i by -1 to reverse the direction of loading

(e) Determine the displacement increments $\{\Delta U_1^i\}$ using Eq. (15)

$$\{\Delta U_j^i\} = \lambda_1^i\{\hat{U}_1^i\} \qquad (20)$$

B. For the subsequent iterations ($j \geq 2$)

(a) Update the global structural stiffness matrix $[K_{j-1}^i]$

(b) Solve the following equations for the displacements $\{\Delta\hat{U}_j^i\}$ and $\{\Delta\overline{U}_j^i\}$ which denote the displacement vector due to reference load vector and unbalanced load vector $\{R_{j-1}^i\}$, respectively

$$[K_{j-1}^i]\{\Delta\hat{U}_j^i\} = \{\hat{P}\} \qquad (21)$$

$$[K_{j-1}^i]\{\Delta\overline{U}_j^i\} = \{\hat{R}_{j-1}^i\} \qquad (22)$$

(c) Determine the load increment parameter λ_j^i by Eq. (12)

(d) Calculate the total displacement increments $\{\Delta U_j^i\}$ for the current iterative step by Eq.

$$\{\Delta U_j^i\} = \lambda_j^i\{\hat{U}_j^i\} + \{\Delta\overline{U}_j^i\} \qquad (23)$$

Step 2: Calculate the total applied load vector $\{P_j^i\}$, total structural displacement vector $\{U_j^i\}$, and the load factory $\{\Lambda_j^i\}$ following equations, respectively.

$$\Lambda_j^i = \Lambda_{j-1}^i + \lambda_j^i \qquad (24)$$

$$\{P_j^i\} = \Lambda_j^i\{\hat{P}\} \qquad (25)$$

$$\{U_j^i\} = \{U_{j-1}^i\} + \{\Delta U_j^i\} \qquad (26)$$

Step 3: Update the shape of the structure considering the displacement increments. For the frame element,

update the section axes and element axis.

Step 4: Calculate the internal forces of the every elements

Step 5: Calculate the internal force vector $\{F_j^i\}$ and unbalance force vector

$$\{R_j^i\} = \{P_j^i\} - \{F_j^i\} \qquad (27)$$

Step 6: Check the numerical convergence.

Step 7: Re-run Steps 2~6 until the satisfied numerical convergence is obtained.

Step 8: Update $i = i+1$ and go to Step 1 for next incremental analysis.

Step 9: If the load factor Λ_j^i is reach to the pre-defined total load factor, stop the analysis.

2.6. Analysis procedure

In the design of cable-stayed bridges, the optimal cable forces should be determined to ensure the structure suffers minimum deformation. Internal forces occur under the dead load condition. For obtaining the optimal cable forces and structural state under the dead load condition, initial shape analysis is generally performed. By performing this special structural analysis, engineers may determine the initial cable forces which ensure minimum deflection under the dead load condition, and find the structural state under the dead load condition. Thus, initial shape analysis should be performed first to consider the structural state under dead load condition, i.e. before live load analysis. In these paragraphs, the procedure of ultimate analysis for completed steel cable-stayed bridges is proposed as a two-step analysis.

2.6.1. Initial shape analysis for considering dead load condition

In order to obtain the minimized deformed structural state under the dead load condition, optimal cable tensile forces should be decided using a rational initial shape analysis method. In this study, the initial force method for initial shape analysis was used to determine the cable tensile forces, and the structural state which allows the
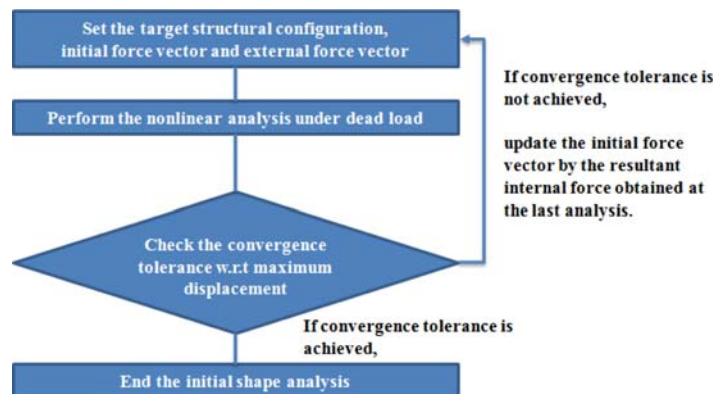

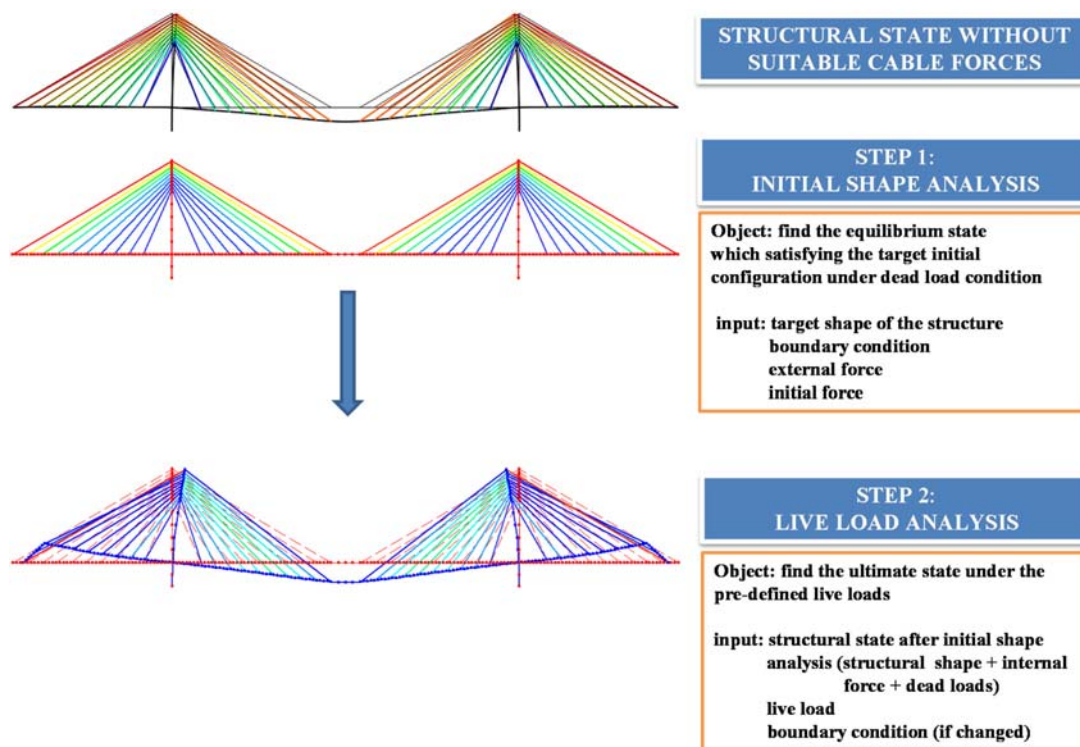**Figure 4.** Procedure of initial shape analysis (initial force method).

Figure 5. Proposed analysis strategy of ultimate analysis for steel cable-stayed bridges.

minimum deformation and bending moment under the dead load condition (Wang *et al*., 1993a; Wang *et al*., 1993b). The following figure presents the analysis sequence of the initial shape analysis, using the initial force method, and the detail procedure is as follow:

Step 1: Set the initial shape (or target shape after the initial shape analysis) of the completed structure with considered initial (initial tension of the cables) and external forces at the analysis stage

Repeat step 2~5 until the deformed structural shape converge to the target shape. (*k* of each term denotes the iteration number of the initial shape analysis.)

Step 2: Set the external and initial force vectors $\{P^k\}$, $\{IF^k\} = \{F^{k-1}\}$, and global stiffness matrix $[K^{k-1}]$

Step 3: Calculate the displacement increments $\{\Delta U^k\}$ by performing the incremental-iterative analysis

Step 4: Update the position vector $\{L^k\} = \{L^{k-1}\} + \{\Delta U^k\}$ and internal force vector $\{F_k\}$

Step 5: Check the structural deformation

The initial shape analysis is iteratively performed following above procedure based on the nonlinear FE analysis procedure described in 2.5.

2.6.2. Analysis strategy of the ultimate analysis for steel cable-stayed bridges

Figure 5 presents the proposed ultimate analysis scheme for steel cable-stayed bridges under various live load conditions. As mentioned previously, the proposed analysis is basically performed as a two-step analysis. In order to

consider the structural state under the dead load condition, the initial shape analysis is performed first. By performing the initial shape analysis first, optimal cable tensile forces are determined and the deformation and internal forces under the dead load condition is found. In this analysis step, only the dead load is considered. Subsequently, the live load analysis of the structure whose static force-equilibrium condition is found by the initial shape analysis is performed, considering material and geometric non-linearities, to trace the ultimate behavior of steel cable-stayed bridges under specific live load cases. All analyses are performed based on the theory of nonlinear finite element analysis.

3. Numerical Analysis Validation

In this section, several analytical examples are introduced for verifying the developed program in this study. Firstly, geometric nonlinear analysis using the nonlinear frame element and nonlinear equivalent truss element are described for verifying the nonlinear elements. After that, elastic/inelastic buckling analysis of the axial member using nonlinear analysis is performed to verify the accuracy and rationality of the algorithm of geometric and material nonlinear analysis.

3.1. Nonlinear analysis for the cantilever beam supported by pre-stressed cable

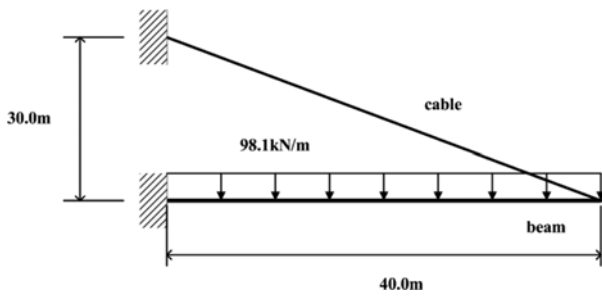In this section, the result of nonlinear analysis for the

Figure 6. Cantilever beam supported by cable member.

Table 1. Geometric and material properties of the structure

	Beam	Cable
Elastic modulus E (kN/m^2)	2.1×10^8	2.1×10^8
Section area A (m^2)	2.0	0.03
2nd moment of inertia I (m^4)	0.04167	-
Weight per unit volume γ (kN/m^3)	77.0 (Not considered)	77.0

cantilever beam supported by pre-stressed cable is introduced to validate the finite elements used in this study. For modeling the cantilever beam, 10 nonlinear frame elements are used, while a nonlinear equivalent truss element is used to model the cable member. As shown in Fig. 6, the distributed load applied to the cantilever beam is 98.1 kN/m, and the pre-tensile force applied to the cable is 1,068 kN. The geometric and material properties of this model are shown in Table 1.

Figure 7 presents the vertical and rotational displacement obtained by nonlinear analysis using the developed program. The displacement components are compared with former research results obtained by analysis using an elastic catenary cable element. It is well known that nonlinear analysis using an elastic catenary cable element can give analytical results that are the closest to the exact solution for cable members. However, if an elastic catenary cable element is

used for modeling the cable member, many calculations need to be made, and made numerous times. As shown in Fig. 7, the two analytical results are almost identical. This similarity occurs because an exact shape function is used to derive the equivalent elastic modulus for considering the cable sag effect. From the comparison, it can be concluded that rational analytical results can be obtained by using this nonlinear equivalent truss element for modeling cable members.

3.2. Inelastic buckling analysis by nonlinear analysis using nonlinear frame elements

One of the main factors that affect the ultimate behavior of steel cable-stayed bridges are material plasticity. There are several ultimate behavior related with material yield as follows:

Material yield of the cable, girder, and masts
Inelastic buckling of the girder, and masts

Firstly, a consideration of the material yield of a cable member is not difficult to do, because the cable is assumed as an axial member. It can easily be analyzed, by comparing the applied axial force with the yield force of the cable member.

Among those factors, nonlinear analysis for tracing the material yield or elastic/inelastic buckling of the girder or mast using beam or frame elements may be relatively difficult, because these beam-column members are subjected to axial force as well as bending moment. If shell elements are used to model a beam-column member, nonlinear analysis may be performed more easily. But much more calculations or analysis time is required when shell elements are used. For efficient nonlinear analysis in this study, the girder and mast are modeled by the nonlinear frame element method, and the refined plastic hinge method is used for considering material nonlinearities. Therefore, the analysis algorithm for elastic/inelastic buckling should be verified through the rational analysis examples.

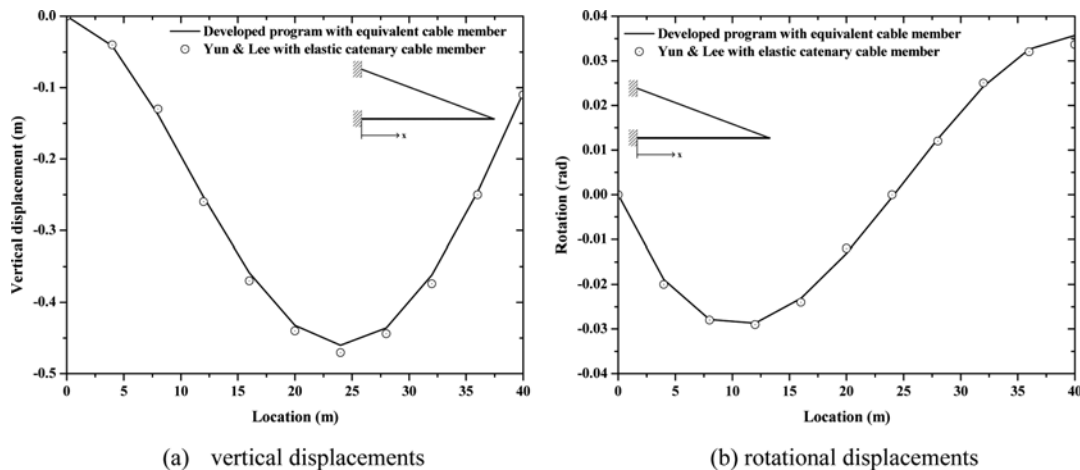In this section, the verification of geometric and material

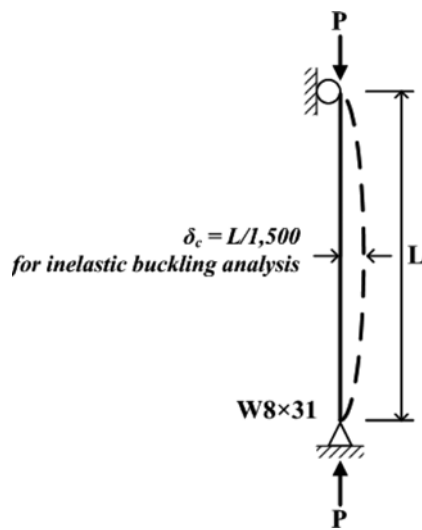| (a) vertical displacements | (b) rotational displacements |

Figure 7. Displacements of the cantilever beam.

Figure 8. Simply supported column with a W8×31 section.

Table 2. Geometric and material properties of the model in Fig. 8

Elastic modulus E (*psi*)	29,000
Section area A (*in.*^{2})	9.12
2nd moment of inertia I_x (*in.*^{4}) (with respect to a weak axis)	37.1
Boundary condition	Simply supported ends
Length of structure L (*in.*)	20.0~280.0
Yield stress f_y (*ksi*)	36.0

nonlinear algorithm is described by the results of inelastic buckling analysis using frame elements. For the analysis, simply supported columns with a W8×31 section and different lengths are used. The column is modeled having an initial imperfection of 2nd order parabolic shape, which

is shown in Fig. 8. The δ_c shown in Fig. 8 is assumed as L/1,500. Table 2 shows the material and geometric properties of the model. The lengths of the columns are designed within the range of the inelastic buckling zone presented by AISC-LRFD specification.

Figure 9 presents the inelastic buckling loads of a simply supported column subjected to axial load, referred to the slenderness parameter λ_c. As shown in the figure, the inelastic buckling loads obtained by nonlinear analysis using the developed program are almost the same as the values obtained by the AISC-LRFD inelastic buckling curve. The range of difference between inelastic buckling loads obtained by the developed program and the AISC-LRFD specification is −4.19 to 2.25%. So, it is proven that inelastic buckling of a member with compressive force can be reasonably solved by the developed program, using frame elements.

4. Ultimate Behavior of Steel Cable-stayed Bridges

4.1. Analysis model

In this chapter, the ultimate behavior of long-span steel cable-stayed bridges under specific live load cases is described in detail. Through the detailed observation of analysis results, governing factors that cause the ultimate behavior of steel cable-stayed bridges were studied and are described in this study. The developed program referred to in previous chapters is used for the ultimate analysis of steel cable-stayed bridges.

Figure 10 shows the analysis models considered in this study. As shown in the figure, basically two different cable-arrangement types are considered. Figure 11 considers the live load cases used in this study. Live load cases that are acting vertically distributed on the girder are designed by
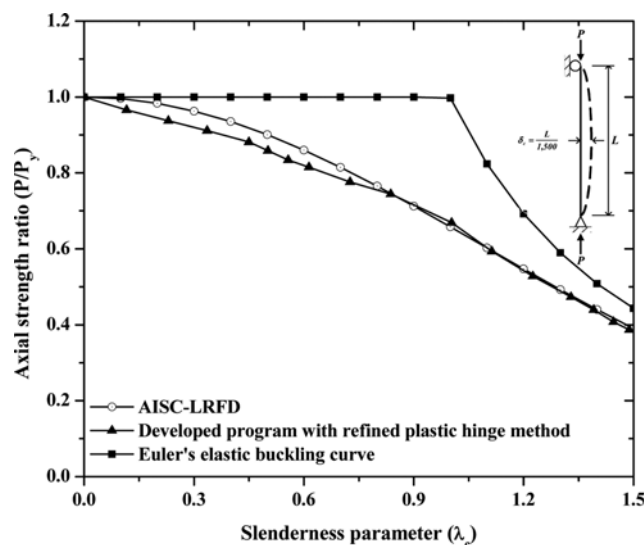

Figure 9. Inelastic buckling load curve (AISC-LRFD inelastic buckling curve/Euler's elastic buckling curve/analysis result by developed program).
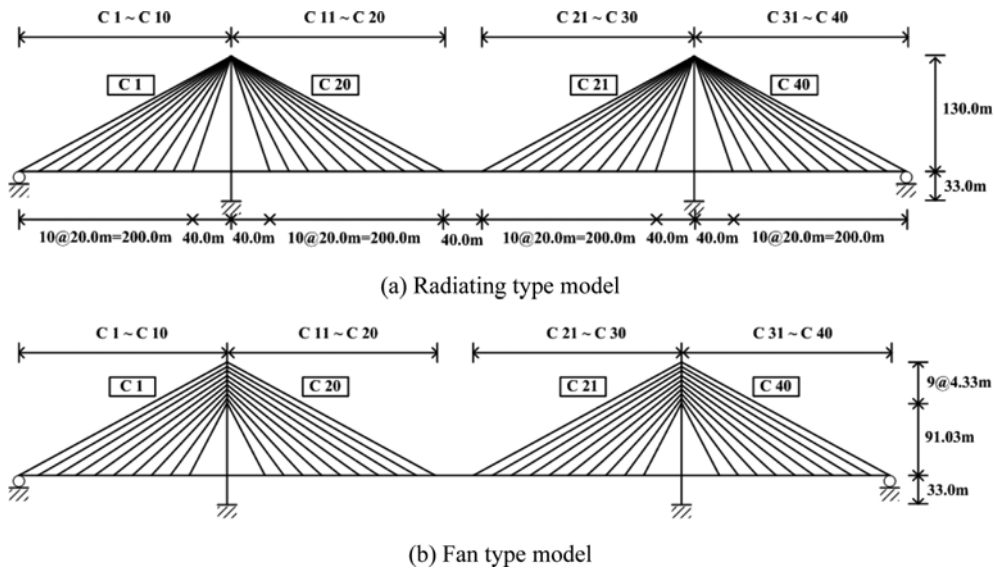
(a) Radiating type model

(b) Fan type model

Figure 10. Analysis model.

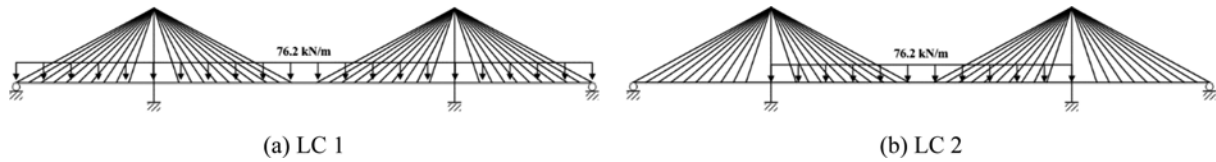(a) LC 1   (b) LC 2

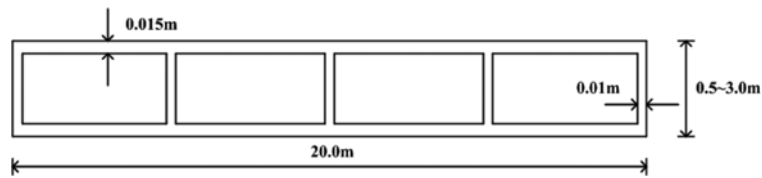**Figure 11.** Considered live load cases.

Figure 12. Section of the girder.

reference to the Korean Specification for Highway Bridges. The live loads assumed by traffic load are a 12.7 kN/m/ lane, and a six-lane road condition is assumed for each bridge. The two live load cases were considered and applied to the girder as shown in Fig 11. Also, deal loads were calculated and applied as the distributed loads considering the unit weigh and sectional area of the girder, masts, and stay cables as shown in Table 3.

As shown in Fig. 12, the girder is designed with a four-cell box. It is assumed that there are sufficient stiffeners and ribs for preventing local buckling in the section. The

section of the mast is designed as a one-cell box, and the same assumption about local failure is adopted.

Table 3 represents the material and geometric properties of the girder, mast, and cables.

4.2. Initial shape analysis

As mentioned previously, cable-stayed bridges are designed with suitable cable tensile forces that ensure the structure suffers minimum deformation under the dead load condition. In general, initial shape analysis is performed to determine the optimal cable tensile forces, and to check the structural state under the condition. So, for more rational analysis, the initial shape analysis should be performed before the live load analysis. The ultimate analysis method proposed in this study includes the step of initial shape analysis. In this section, the analysis results of initial shape analysis are briefly presented.

Figure 13 shows the decrease of the maximum deflection of the girder as the repeated initial shape analysis is performed. The assumed maximum allowed vertical
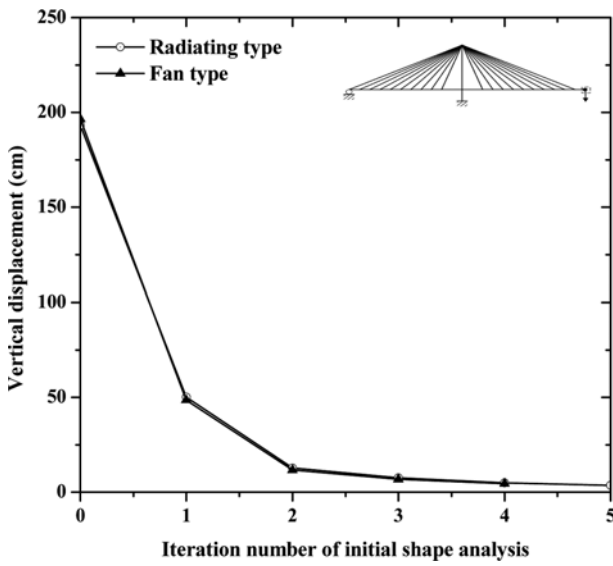
Table 3. Material and geometric properties of main members

	Girder	Mast	Cable
Elastic modulus E (kN/m^2)	2.1×10^8	2.1×10^8	2.1×10^8
Sectional area A (m^2)	0.75	0.79~0.86	0.02
2nd moment of inertia I (m^4)	1.45	3.14-8.21	-
unit weight γ (kN/m^3)	218.27	76.90	76.90
yield stress f_y (MPa)	380.0	Elastic	1,800.0

Figure 13. Decrease of the maximum deflection by the repeated initial shape analysis (A_g=0.75 m², I_g=1.45 m⁴, A_m=0.79 m², I_g=3.14 m⁴, A_c=0.02 m²).

deflection is 0.01% of the center span length. After several repeated analyses, the maximum deflection of the radiating type model and fan type model are 3.59 and 4.50 cm, respectively. (The maximum horizontal displacements of the radiating type model and fan type model are 0.18 and 0.37 cm, respectively.) According to the results of the decrease of maximum deflection, it can be concluded that the initial shape analysis used in this study can find suitable cable tensile forces, which ensure the structure suffers minimum deflection under the dead load condition.

Figure 14 shows the distribution of the tensile force of cables obtained by initial shape analysis. Tensile forces of cables are required to resist vertical loads applied to the girder and cables. Because the total weights of both two models are almost the same, the vertical components of cables in each model are also almost the same. In contrast, there is a difference in the comparison of horizontal components of the stay cables. Although the required vertical components of tensile forces are almost the same, the required resultant cable forces should differ, because the cable arrangement type is different. In order words,
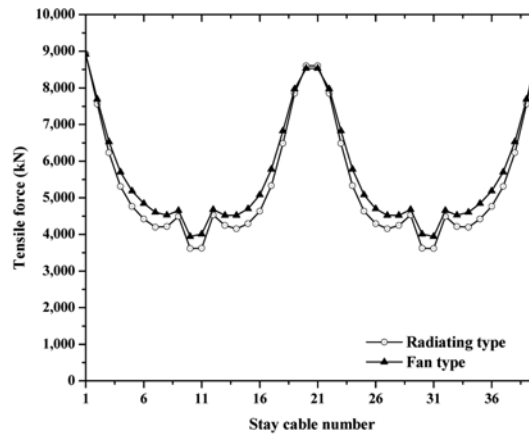
(a) resultant forces
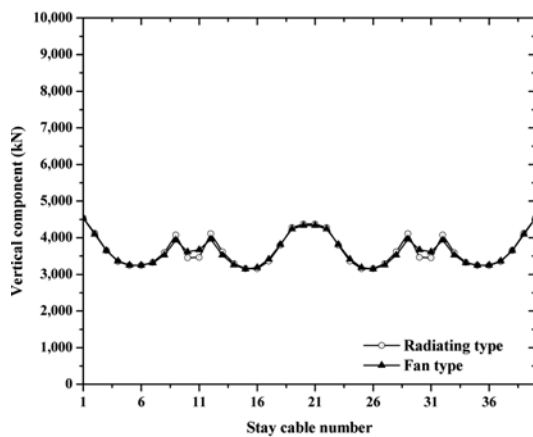
(b) vertical components
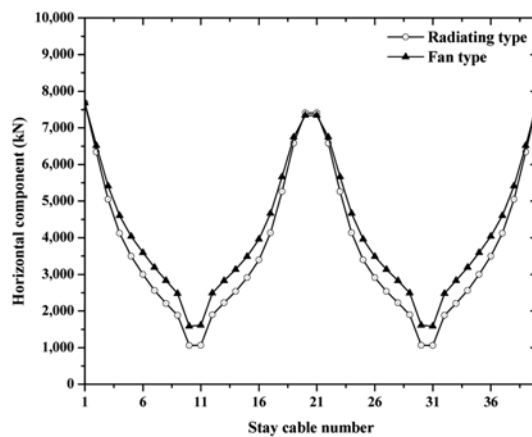
(c) horizontal components

Figure 14. Tensile force of cables after the initial shape analysis.
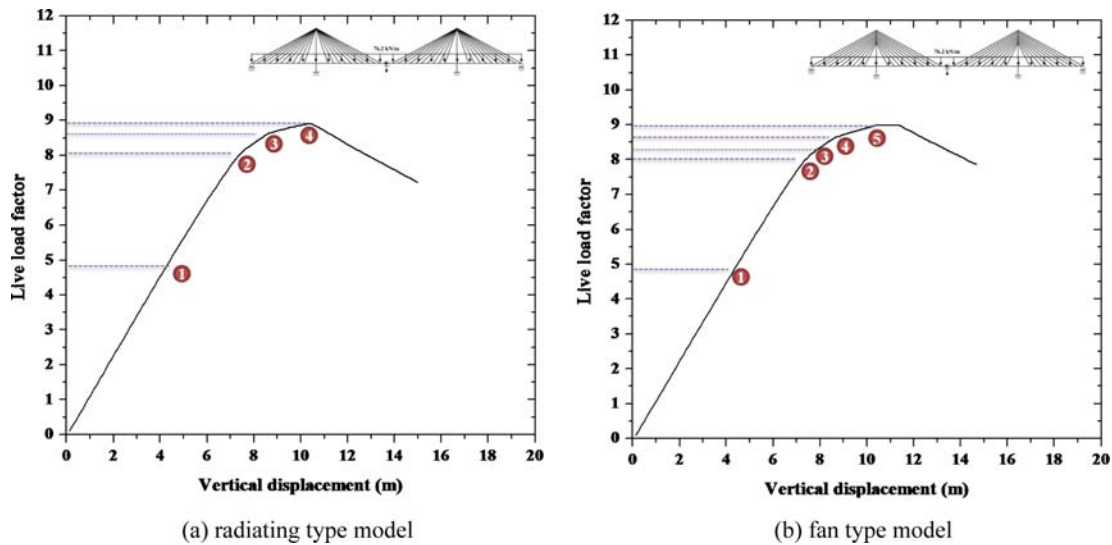
(a) radiating type model

(b) fan type model

Figure 15. Load-displacement curve under LC1.

the horizontal angle of stay cables of the radiating type model is larger than the horizontal angle of stay cables of the fan type model, so the required resultant cable forces of the radiating type model is smaller than the forces of the fan type model. Further, for the same reason, the horizontal components of cable forces of the radiating type model are also smaller than the components of cable forces of the fan type model. In summary, when the horizontal angles of stay cables are lower, larger cable forces are required, and the girder is subjected to larger compressive forces under the dead load condition.

4.3. Ultimate behavior under vertically applied live load

In this chapter, the general ultimate behavior under the vertically applied live load shown in Fig. 13 is described. In former researches, these live load conditions were

dealt with as main live load cases, but detailed behavior characteristics under these load cases have not been described. With decisive analysis results, the general ultimate behavior of completed steel cable-stayed bridges can now be presented in detail.

4.3.1. Ultimate behavior under the vertically distributed load acting on the whole span, LC1

In this section, the ultimate behavior under a distributed load acing on the whole span is described. Figure 15 presents the load-displacement curves at the center of the center span of each model under LC1. As shown in Fig. 15, there are obvious ultimate points. After the live load factor reaches the ultimate point, which is the ultimate live load factor, the load factor starts to decrease with continuous increase of deformation.
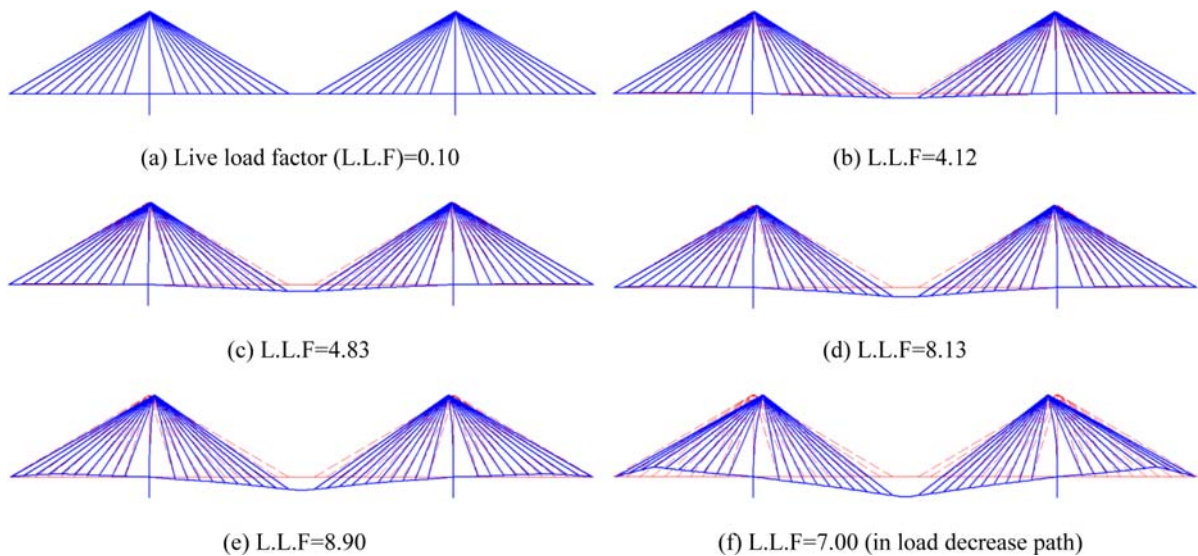

(a) Live load factor (L.L.F)=0.10

(b) L.L.F=4.12

(c) L.L.F=4.83

(d) L.L.F=8.13

(e) L.L.F=8.90

(f) L.L.F=7.00 (in load decrease path)

Figure 16. Deformed shape of the radiating type model under LC 1 (scale factor: 2.0)

(a) L.L.F=0.01

(b) L.L.F=4.14

(c) L.L.F=4.87

(d) L.L.F=8.05

(e) L.L.F=8.99

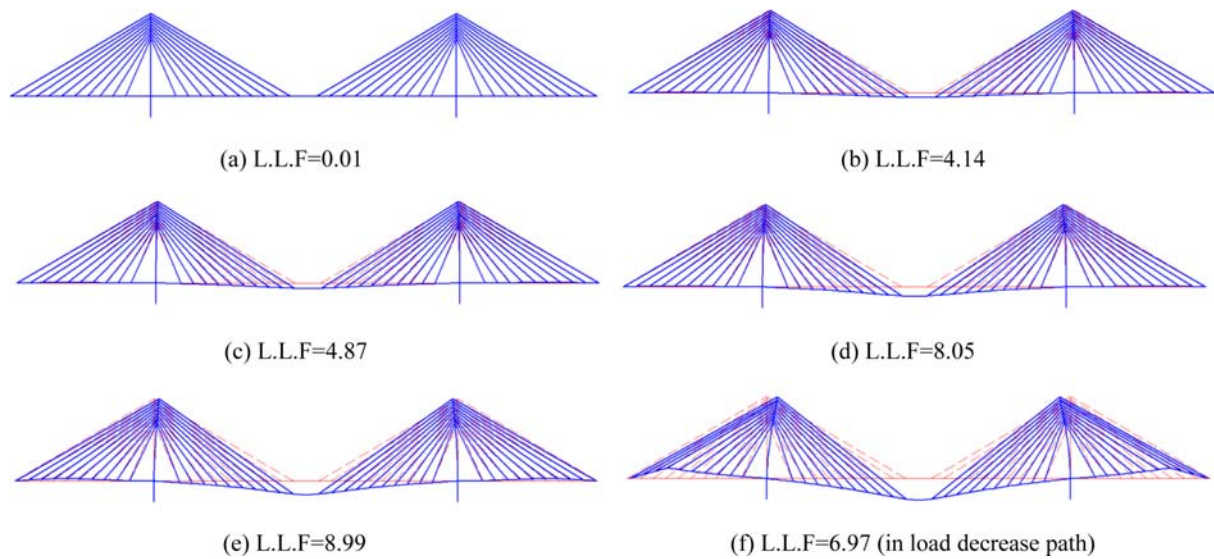(f) L.L.F=6.97 (in load decrease path)

Figure 17. Deformed shape of the fan type model under LC 1 (scale factor: 2.0).

Figures 16 and 17 show the deformed shapes under LC1. Under the vertically distributed load acting on the whole span, the center span shows continuous downward deformation, while both side spans show upward deformation. When the external force is applied to the whole span, tensile forces of the cables increase to resist a deflection of the girder. Because the lengths of side span and half of the center span are different, the summation of the required vertical components of the ten cables of one side span is different to the summation of the required vertical components of the ten cables which hang on the same mast, but which support the center span. So, each mast is subjected to horizontal force because of the resultant of cable forces, and these horizontal forces make each mast suffer flexural deformation, with horizontal displacements toward the center of the structure. As each mast suffers flexural deformation with horizontal displacement, each side span suffers uplift, a type of flexural deformation,

Table 4. Events of the radiating type model during LC1 increases

Live load factor	Event
4.83 (1)	First plastic hinge occurs at the section of girder near the junction between girder and mast.
8.13 (2)	Second plastic hinge occurs at the center of center span girder. Exterior cables, C1 and C40, yield.
8.63 (3)	C2 and C39 yield.
8.90 (4)	Due to excessive negative bending moment, additional plastic hinges -occur at the section supported by C4 and C37 in both side spans. Load decrease starts.

Table 5. Events of fan type model during live load LC1 increases

| Live load factor	Event
4.87 (1)	First plastic hinge occurs at the section of girder near the junction between girder and mast.
8.05 (2)	Second plastic hinge occurs at the center of center span girder.
8.21 (3)	Exterior cables, C1 and C40, yield.
8.68 (4)	C2 and C39 yield.
8.90	Due to excessive bending moment and the largest compressive force, -plastic hinges occur at sections supported by C10 and C31 in both side spans.
8.98	C3 and C38 yield.
8.99 (5)	Due to excessive negative bending moment, additional plastic hinges occur -at the section supported by C4 and C37 in both side spans. Load decrease starts.

(a) side span cables   (b) center span cables
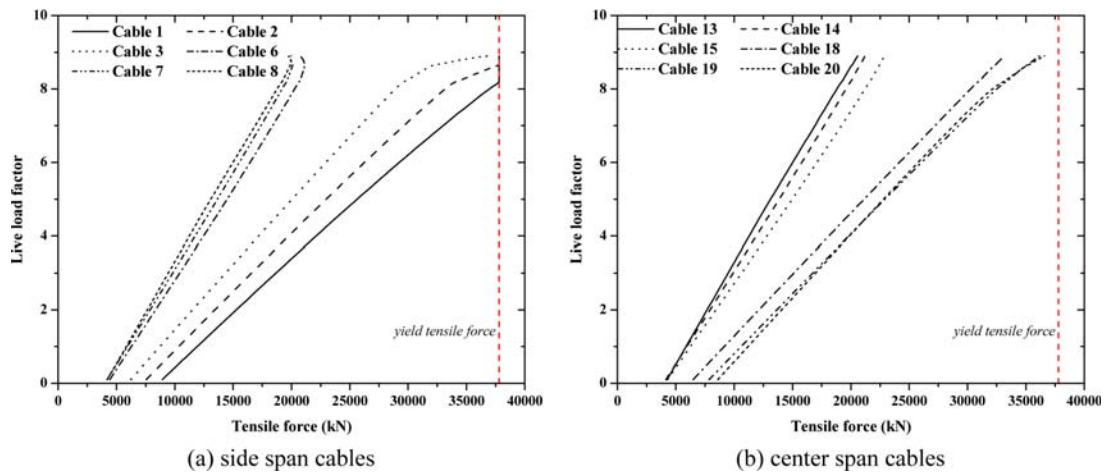
Figure 18. Cable tensile forces of the radiating type model under LC 1.

(a) side span cables   (b) center span cables
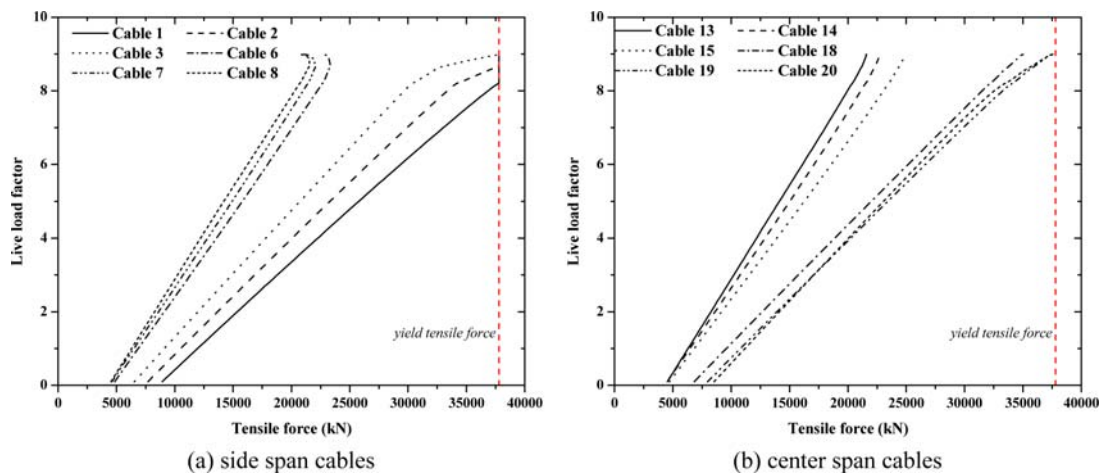
Figure 19. Cable tensile forces of the fan type model under LC 1.

because of the stay cables. The flexural deformation of both side spans is amplified by the compressive forces induced by the stay cables. Because of these causes, the upward deformation increases as the external load increases, although both side spans are also subjected to the vertically distributed load.

The significant events that occur during the structure reaching its ultimate state are presented in Tables 4 and 5. Also, live load factors of each event are indicated together. First, a material yield section is revealed at the junction between the girder and mast. This section is subjected to the largest compressive force in the girder. Because of excessive compressive force with negative moment, the first plastic hinge occurs at this section. As the external force increases, an additional plastic hinge occurs at the center of the center span. In this section, the largest positive bending moment and tensile force occur together. After that, with continued increase of the external force, several stay cables yield, and global structural deformation also increases. As negative flexural deformation is amplified by the beam-column effect at both side spans, some

sections in both side spans yield because of excessive negative bending moment with compressive forces induced by stay cables. After additional plastic hinges occur, the structure reaches its ultimate state, and the external load factor starts to decrease.

Figures 18 and 19 show the load-cable force curves under LC 1. As shown in these figures, significant nonlinear responses of the load-cable force relationship are not evident. Each cable suffers increasing force, because of continued global deformation of the structure. Considering the previous global behavior under LC1, the force increase of stay cables in the center span is due to the downward deformation of the center span, while the force increase of stay cables in the side span is due to the flexural deformation of the mast itself, and the uplifting action of the mast.

In this section, the ultimate behavior under LC1 was described. For LC1, ultimate live loads factors of the assumed FE models in this study were 8.90 and 8.99, respectively. Although the horizontal angle of stay cables of the radiating type model is higher than that of the fan
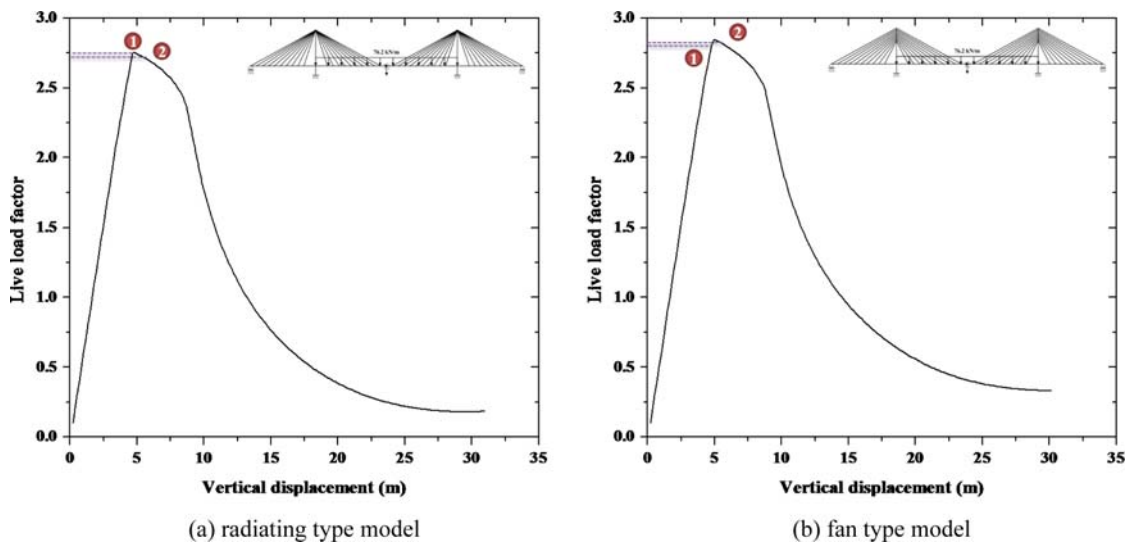
(a) radiating type model   (b) fan type model

Figure 20. Load-displacement curve under LC2.

type model, the ultimate live load factor is lower than the value of the fan type model.

Consequently, the external load factor starts to decrease when plastic hinges occur at the side span because of excessive negative flexural deformation. The flexural deformation is made and amplified by the beam-column effect. There are several factors that may affect this behavior of the beam-column effect of the girder. These factors are described in the next chapter, and the reason why the radiating type model shows a lower ultimate capacity under these live load cases is also introduced.

4.3.2. Ultimate behavior under the vertically distributed load acting on the center span, LC2

In this section, the ultimate behavior under the vertically distributed load acing on only the center span is described. Figure 20 represents the load-displacement curves at the center of the center span of each model under LC2.

Similar to the behavior under LC1, there is a significant ultimate point in the load-displacement curve under LC2. After the live load factor reaches its highest point, the factor starts to decrease with continuous increase of deformation, which means an inverse stiffness state. Figures 21 and 22 show the deformed shapes under LC2.

When the vertically distributed load is applied to only the center span, vertical deflection occurs at the center span first. As the center span suffers vertical deflection, both masts also suffer flexural deformation, with horizontal movement toward the center of the structure, because of interaction between the girder-mast-stay cables. The horizontal movement of the mast leads to the uplift of both side spans, because both side spans are also connected with the mast by stay cables. As the external load increases, more horizontal movement of the mast occurs, and the uplifting of the side spans also increases. By the way, the side span has been subjected to compressive

forces induced by stay cables. So, the flexural deformation is amplified due to the compressive force and it makes for a significant beam-column effect of the girder of the side span. The deformed shapes under LC2 are very similar with those under LC1. But, under LC2, each mast is subjected to larger horizontal forces, because only the center span is subjected to the vertical forces. Moreover, inverse flexural deformation, which means upward deformation, hasn't been controlled by the vertically distributed external load applied to the side spans under LC2. Therefore, under LC2, negative bending moment at the side span increases faster, and critical sections of both side spans yield by a quite lower live load factor than the value under LC1.

Figures 23 and 24 show the load-cable force curves under LC2. In this figure, there is an interesting tendency of these curves for stay cables that support both side spans. As the external force increases, tensile forces of cables near the mast decrease. In addition, tensile forces of cable 3 and cable 4 also decrease after the structure reaches its ultimate state. This is caused by shortening of the straight-line distance of stay cables. When the straight-line distance of a stay cable is shortened, the tensile force of the cable is reduced. As shown in Figs. 21 and 22, and also mentioned previously, upward deformation of the side spans occurs when external force is applied to the center span. Further, the upward deformation is amplified by the beam-column effect of the side span. If the uplifting effect by the horizontal movement of the mast mainly affects the upward deformation, cable tensile forces of stay cables in the side span may continuously increase. But the beam-column effect, amplified by compressive forces, mainly affects upward deformation of the side span. The decrease of tensile forces of stay cables can be evidence of this behavior. In addition, negative bending moment of the side span grows rapidly and are widely
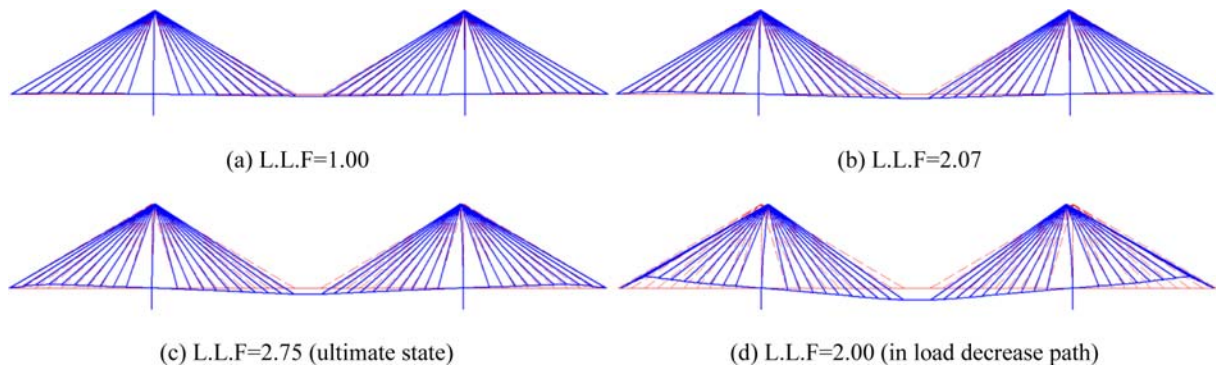
(a) L.L.F=1.00   (b) L.L.F=2.07

(c) L.L.F=2.75 (ultimate state)   (d) L.L.F=2.00 (in load decrease path)

Figure 21. Deformed shapes of the radiating type model under LC2.

(a) L.L.F=1.00   (b) L.L.F=2.05

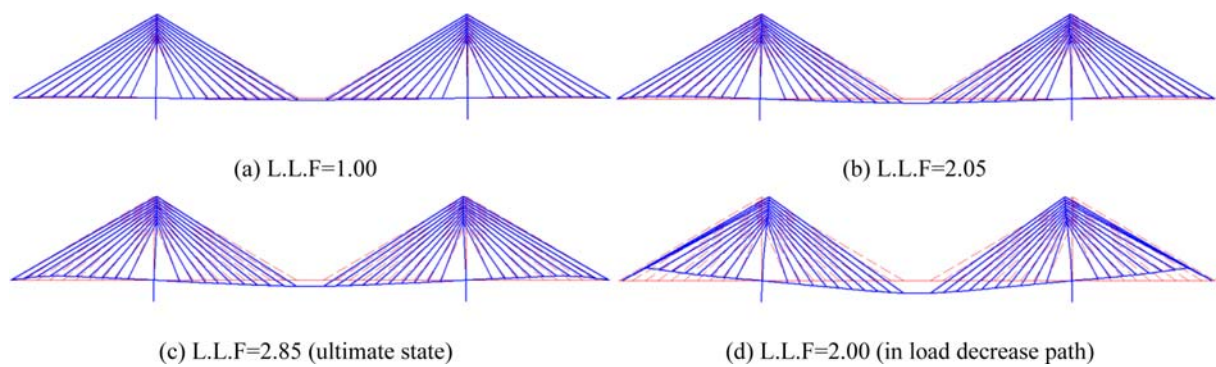(c) L.L.F=2.85 (ultimate state)   (d) L.L.F=2.00 (in load decrease path)

Figure 22. Deformed shapes of the fan type model under LC2.

distributed, because stay cables in the side span can't resist the upward deformation induced by the amplified beam-column effect, although the cables are basically designed as intermediate supports. Consequently, the structure reaches its ultimate state at quite a lower load level under LC2 (compared with ultimate live load factor under LC1), although LC2 is applied only to the center span.

Figures 25 and 26 show the change of bending moment distribution as the external force changes. As the upward deformations of both side spans increases due to the amplified beam-column effect, negative bending moments are distributed widely in both side spans. Because a cable

can't resist the compressive behavior, stay cables can't function as intermediate supports for the side span, which suffers upward deformation due to the beam-column effect. Therefore, negative bending moments are distributed mainly in side spans when the structure reaches its ultimate state.

As shown previously in regard to ultimate behavior obtained by ultimate analysis, the fan type model shows a larger ultimate live load factor, (which means an ultimate capacity under both live load cases, LC1 and LC 2), than the radiating type model. For those live load cases, the structure reaches its ultimate state by excessive

Table 6. Events of the radiating type model during LC2 increases

Live load factor	Event
2.75	Due to excessive negative bending moment, the first plastic hinge occurs -at the section supported by cables 3 and 38 in both side spans. Load decrease starts.
2.73	Exterior cables, C1 and C40, yield.

Table 7. Events of the fan type model during LC2 increases

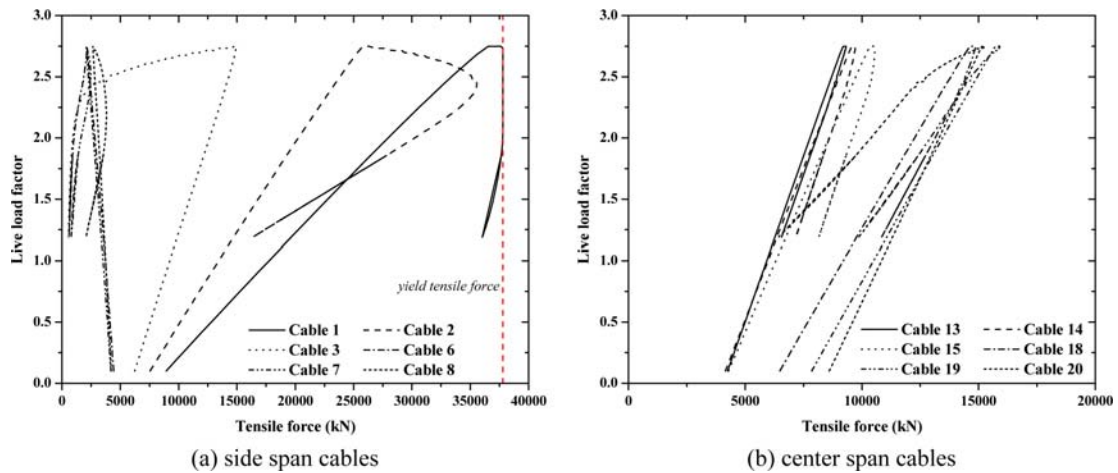| Live load factor	Event
2.80	Due to excessive negative bending moment, the first plastic hinge occurs -at the section supported by cables 3 and 38 in both side spans.
2.85	Load decrease starts.
2.82	Exterior cables, C1 and C40, yield.

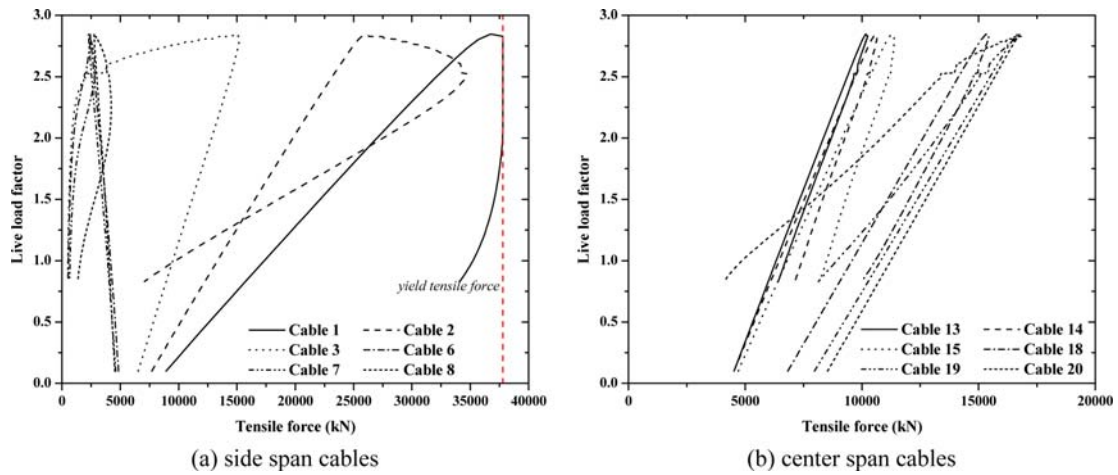**Figure 23.** Cable tensile forces of the radiating type model under LC 2.

Figure 24. Cable tensile forces of the fan type model under LC 2.

upward flexural deformation of both side spans. In other words, after a plastic hinge occurs at the point near the end of the side span, the structure shows its ultimate state. The occurrence of a plastic hinge is relative to the upward deformation of the side spans. There are two factors that affect the upward deformation of a side span; the first is the initial uplift effect by horizontal movement of the mast, and the second is the applied compressive force due to stay cables. The amount of initial uplift of the radiating type model is larger than that of the fan type model, because the horizontal angles of stay cables in the radiating type model are larger. But the compressive force acting on the side span in the fan type model is larger. Those two effects are quite relative to the stay angle of the cables. In general, it is well known that a larger horizontal angle of stay cables leads to better structural efficiency, because smaller compressive forces are acting on the girder. But, it is hard to be conclusive, simply because there are various effect factors on the structural response, as well as induced compressive forces. So, more study of the effect of various factors on global structural response

and ultimate behavior should be performed.

4.4. Comparison with the results obtained by geometric nonlinear analysis

In this chapter, analytical results by nonlinear analysis considering only geometric nonlinearities are introduced. In general, cable-stayed bridges are treated as a "slender structure", because of their geometric characteristics. Moreover, the girder and mast of cable-stayed bridges are subjected to quite large compressive forces that are induced by the stay cables. So, structural stability is also a main concern. In this section, analytical results obtained by geometric nonlinear analysis and ultimate nonlinear analysis are compared, in order to investigate the factor that most affects the ultimate behavior.

As shown in Fig. 27, there are big differences in the peak points obtained by the two analysis methods. While the live load factor increases until the slope of curve obtained by ultimate analysis changes, both curves are almost the same. Slope change occurs when the plastic hinge occurs at the center of the center span. Also, the
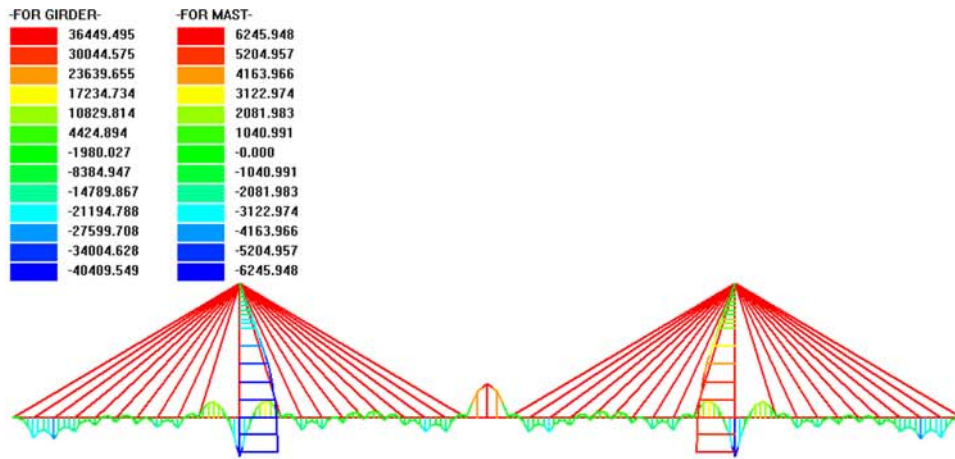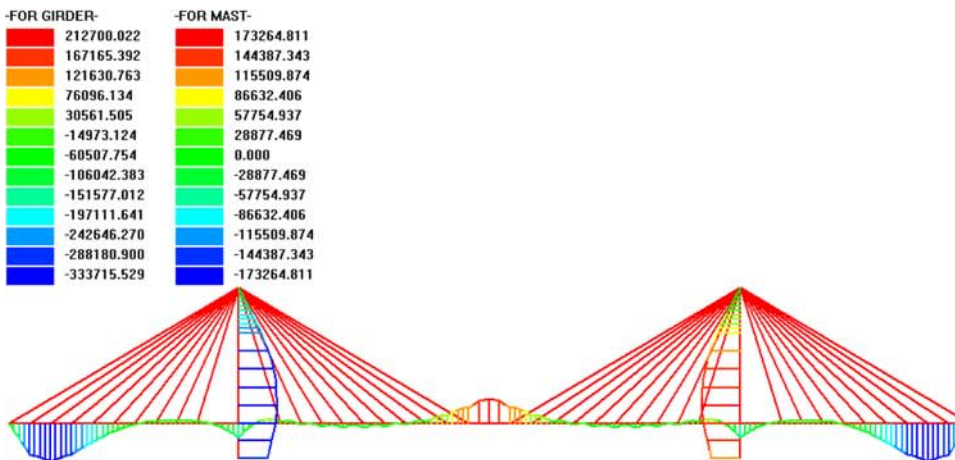
(a) L.L.F: 0.10

(Maximum/minimum bending moment of the girder: 36,449.5/-40,409.5 kN·m)
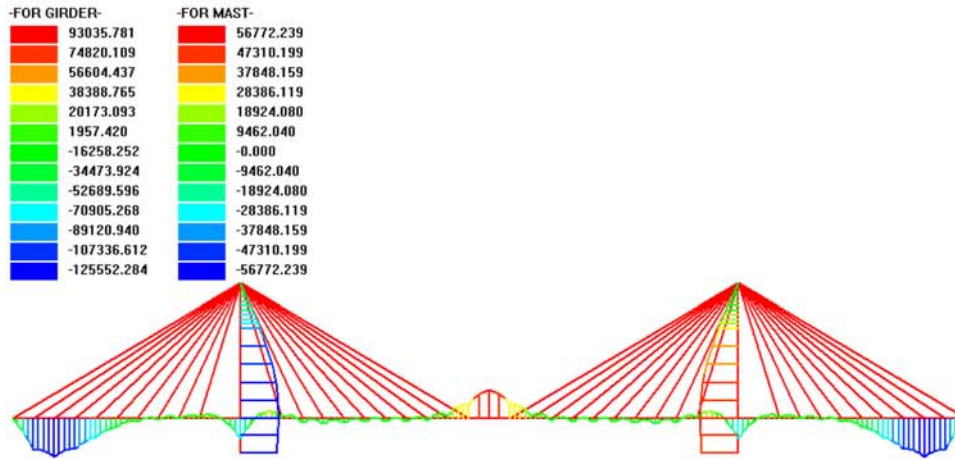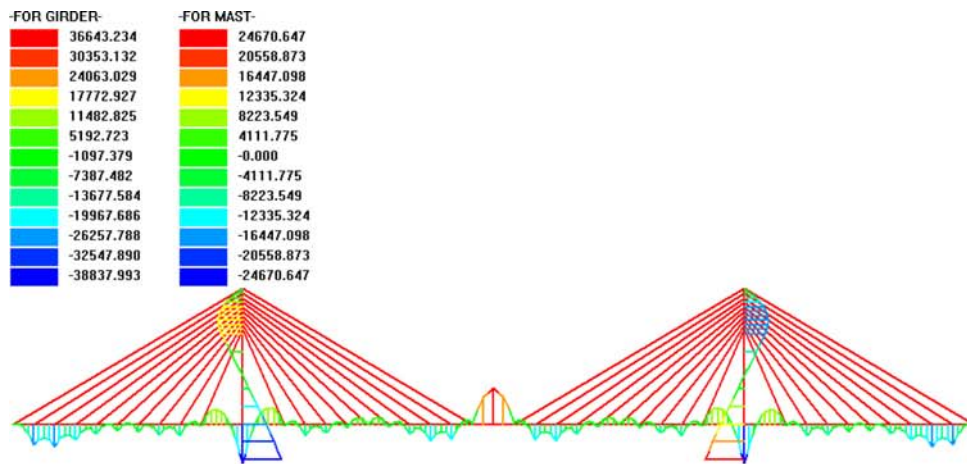

(b) L.L.F: 1.00

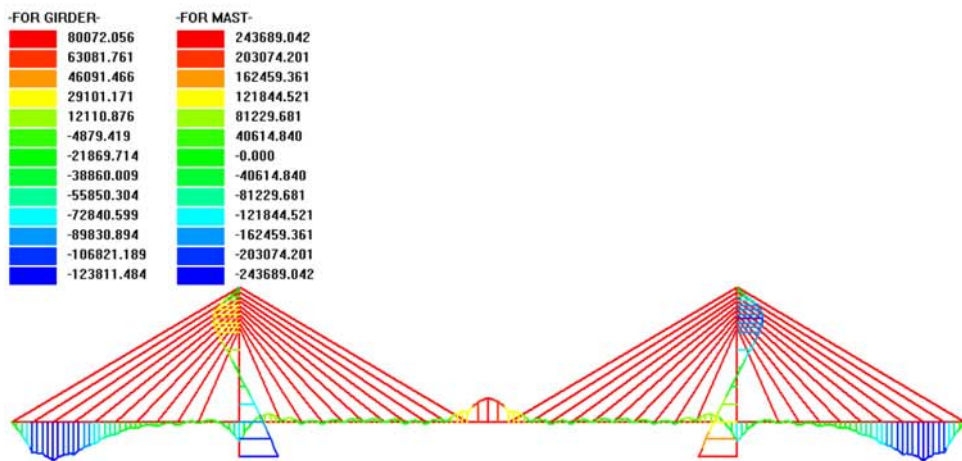(Maximum/minimum bending moment of the girder: 93,035.8/-125,552.3 kN·m)

(c) L.L.F: 2.75

(Maximum/minimum bending moment of the girder: 212,700.0/-333,715.5 kN·m)

Figure 25. Change of the bending moment distribution of the radiating type model.
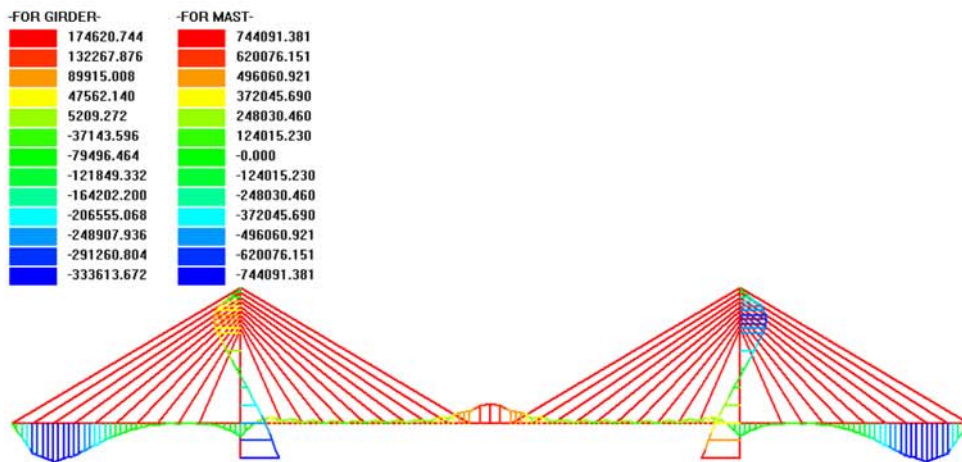
(a) L.L.F: 0.10

(Maximum/minimum bending moment of the girder: 36,643.3/-38,838.0 kN·m)

(a) L.L.F: 0.10

(Maximum/minimum bending moment of the girder: 80,072.1/-123,811.5 kN·m)

(c) L.L.F: 2.85

(Maximum/minimum bending moment of the girder: 174,620.7/-333,613.7 kN·m)

Figure 26. Change of the bending moment distribution of the fan type model.
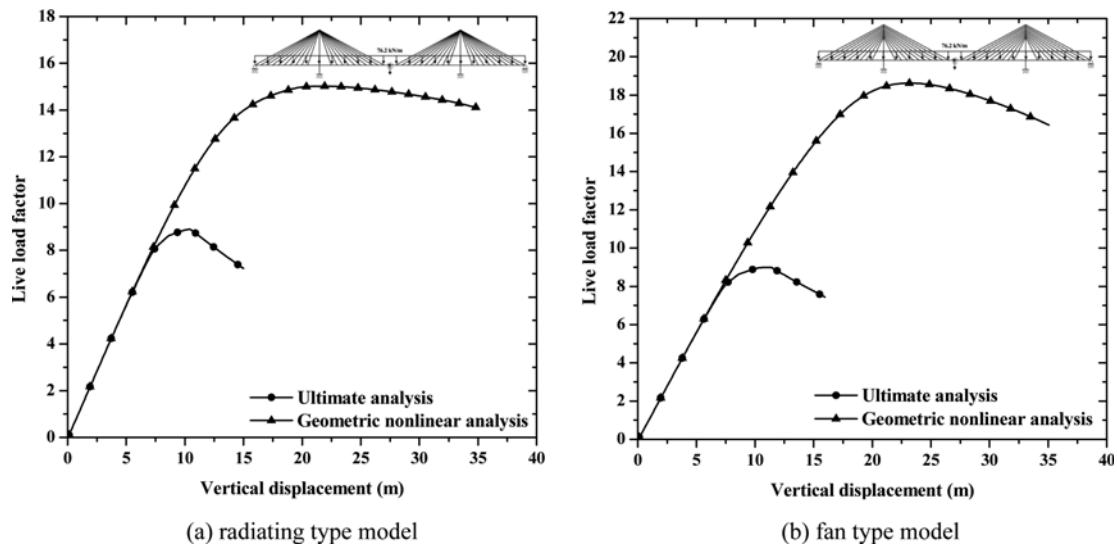
(a) radiating type model   (b) fan type model

Figure 27. Comparison of the load-displacement curves under LC1.

(a) Radiating type (L.L.F: 13.70 in load decrease path)   (b) Fan type (L.L.F: 15.58, in load decrease path)
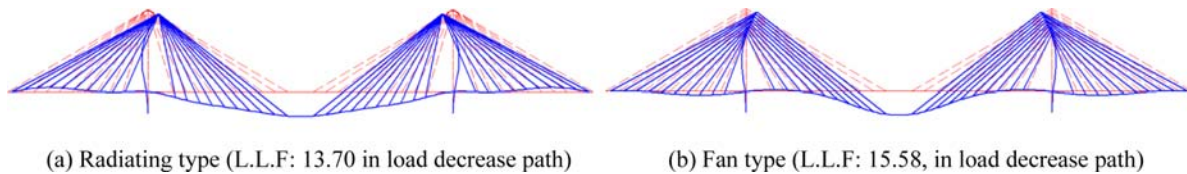
Figure 28. Deformed shapes under LC1 (obtained by geometric nonlinear analysis).

live load factor starts to decrease when the additional plastic hinge occurs at the side span, due to excessive negative flexural deformation. But, the effect of material nonlinearities can't be considered when geometric nonlinear analysis is performed. According to the result by geometric nonlinear analysis, the structure becomes unstable due to the elastic buckling of the girder and mast. The deformed shape for the structural instability obtained by geometric nonlinear analysis is introduced in Fig. 28.

Under LC2, there are similar comparison results. Because the material nonlinearity is not considered when geometric nonlinear analysis is performed, the structure becomes unstable due to elastic buckling of the side span, which is possible if the girder is quite slender. If the member is slender, the member may buckle due to applied compressive forces without material yield, and there may be no difference between the structural responses obtained by geometric nonlinear and ultimate nonlinear analyses. But, for the analysis model designed in this study, the section in the side span yields due to excessive negative bending moment with compressive force, before the side span buckles, as shown in Fig. 30.

Figure 31 shows a comparison of the peak load factors obtained by ultimate analysis and geometric nonlinear analysis. As mentioned previously, the peak load factor obtained by ultimate analysis was smaller than the factors obtained by geometric nonlinear analysis, because of material yield.

According to the results of the comparison, material nonlinearities mainly affect the ultimate behavior of steel cable-stayed bridges. But, it can be said that many geometric nonlinearities also affect the ultimate behavior, such as the beam-column effect of the girder and mast, and the interaction between girder-mast-cable. For example, the interaction between girder-mast-cable causes global interactive deformation of the structure. When vertical force is applied to the center span, the side span suffers upward deformation. This is caused by uplifting due to horizontal movement of the mast, and horizontal movement of the mast is also induced by the vertical deflection of the center span. Further, the upward deformation of the side span is amplified, due to the beam-column effect. Excessive upward deformation also causes an excessive negative bending moment. Therefore, these geometric nonlinearities accelerate structural response, and when the structure reaches the material limit, the structure finally reaches its ultimate state.

Also, there is an interesting point regarding the ultimate or critical live load factor for steel cable-stayed bridges. The ultimate load factor under LC 2 is lower than under LC1. Actually, LC2 is the applied force acting on the center span only. Under LC1 and LC2, excessive upward deformation of the side span makes the structure reach its ultimate state. By the way, under LC2, side spans aren't directly subjected to vertically distributed force. The deformation of side spans is induced by the uplifting
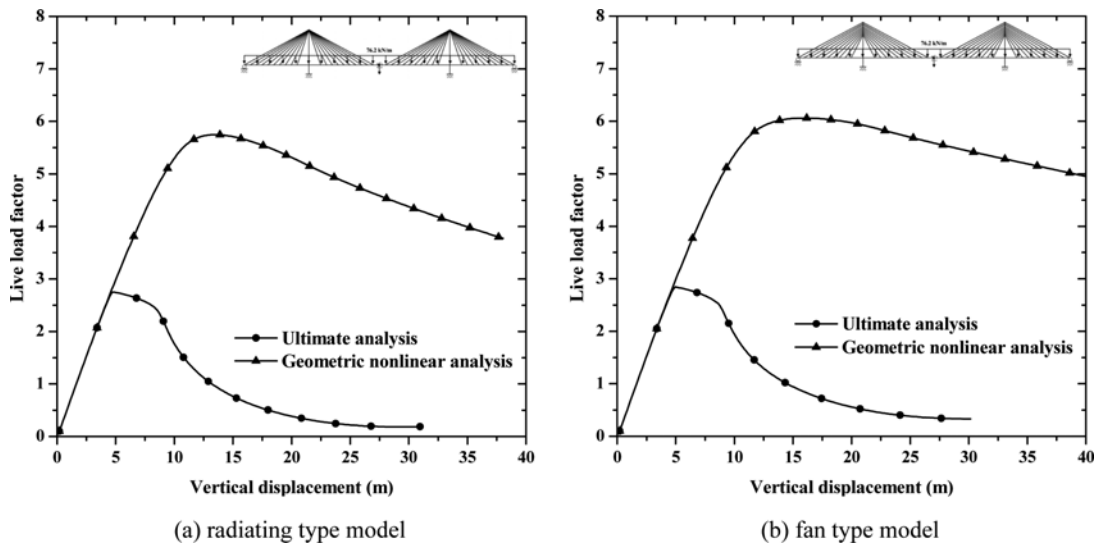
(a) radiating type model   (b) fan type model

Figure 29. Comparison of load-displacement curves under LC2.

(a) Radiating type (L.L.F: 4.88, in load decrease path)   (b) Fan type (L.L.F: 5.83, in load decrease path)
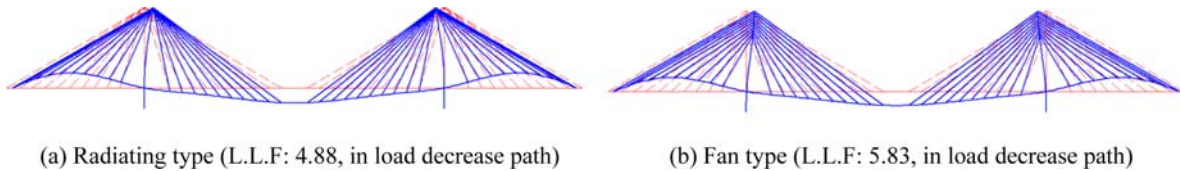
Figure 30. Deformed shapes under LC2 (obtained by geometric nonlinear analysis).

effect, due to the horizontal movement of the mast with compressive forces applied by stay cables. This is a very interesting structural characteristic of cable-stayed bridges. These structural characteristics are exhibited in cable-stayed bridges because of the girder-mast-cable connection and interaction. Under LC1, vertically applied force acting on the side span resists the upward deformation of the side span, so the negative bending moment in the side span increases more slowly than under LC2.

5. Conclusion

This study addresses the ultimate behavior of steel cable-stayed bridges under vertically applied live load cases. In order to rationalize analytical study, a two-step ultimate analysis method was proposed, considering various geometric and material nonlinearities. The two-step ultimate analysis includes initial shape analysis for rationally considering the structural state under the dead load condition and live load analysis. The ultimate behavior of completed steel cable-stayed bridges under vertically distributed load cases was investigated using the proposed analysis method and program. According to analytical studies, it was revealed that the material yield of the girder mainly affects to the ultimate state of steel cable-stayed bridges. Further, material yield occurs as excessive deformation increases at the girder. The deformation basically occurs, and is
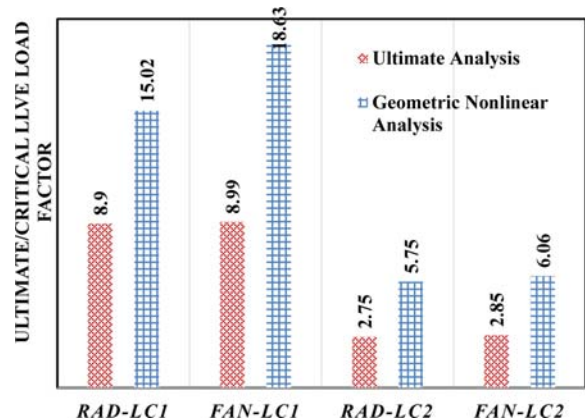

Figure 31. Comparison of ultimate/critical load factor obtained by ultimate analysis/geometric nonlinear analysis.

amplified, by various geometric nonlinearities, such as girder-mast-cable connectivity interaction, beam-column effect of flexural members, and large deformation effect. It can be concluded that these geometric nonlinearities accelerate a structural response; and when the structure reaches its material limit, the structure finally reaches its ultimate state. In this study, limited analysis models were considered. So, more intensive analytical studies are required of the various parameters that need to be considered by the rational ultimate analysis method.

Acknowledgments

References

Adeli, H. and Zhang, J. (1994). "Fully nonlinear analysis of composite girder cable-stayed bridges." *Computers & Structures*, 54(2), pp. 267-277.

Chen, D. W., Au, F. T. K., Tham, L. G., and Lee, P. K. K. (2000). "Determination of initial cable forces in prestressed concrete cable-stayed bridges for given design deck profiles using the force equilibrium method." *Computers & Structures*, 74, pp. 1-9.

Cheng, J. and Xiao, R. C. (2004). "Probabilistic determination of initial cable forces of cable-stayed bridges under dead loads." *Structural Engineering and Mechanics*, 17(2), pp. 267-279.

Crisfield, M. A. (1983). "An arc-length method including line searches and accelerations." *International Journal for Numerical Methods in Engineering*, 19, pp. 1269-1289.

Ernst, H. J. (1965). "Der e-modul von seilen unter berucksichtigung des durchanges." *Der Bauingenieur*, 40, pp. 52-55 (in German).

Fleming, J. F. (1965). "Nonlinear static analysis of cable-stayed bridges." *Computers & Structures*, 10, pp. 621-635.

Freire, A. M. S., Negrao, J. H. O., and Lopes, A. V. (2006). "Geometric nonlinearities on the static analysis of highly flexible steel cable-stayed bridges." *Computers & Structures*, 84, pp. 2128-2140.

Gimsing, N. J. (1965). *Cable supported bridges Concept & Design. 2nd Edition,* John Wiley & Sons Ltd., New-York.

Kim, K. S. and Lee, H. S. (2001). "Analysis of target configurations under dead loads for cable-supported bridges." *Computers & Structures*, 79, pp. 2681-2692.

Kim, S. (2010) *Ultimate analysis of steel cable-stayed bridges*. Ph.D. Dissertation, Korea University, Seoul, Korea.

Lim, N. H., Han, S. Y., Han, T. H., and Kang, Y. J. (2008) "Parametric study on stability of continuous welded rail track -ballast resistance and track irregularity-." *International Journal of Steel Structures*, 8(3), pp. 171-181.

Liew, J. Y. R., White, D. W., and Chen, W. F. (1993). "Second order refined plastic-hinge analysis for frame design. Part I." *Journal of Structural Engineering*, 119(9), pp. 3196-3216.

Ren, W. X. (1999). "Ultimate behavior of long-span cable-stayed bridges." *Journal of Bridge Engineering*, ASCE, 4(1), pp. 30-36.

Shu, H. S. and Wang, Y. C. (2001). "Stability analysis of box-girder cable-stayed bridges." *Journal of Bridge Engineering*, ASCE, 6(1), pp. 63-68.

Song, M. K., Kim, S. H., and Choi, C. K. (2006). "Enhanced finite element modeling for geometric non-linear analysis of cable-supported structures." *Structural Engineering and Mechanics*, 22(5), pp. 575-597.

Song, W. K. and Kim, S. E. (2007). "Analysis of the overall collapse mechanism of cable-stayed bridges with different cable layouts." *Engineering Structures*, 29, pp. 2133-2142.

Tang, C. C., Shu, H. S., and Wang, Y. C. (2001). "Stability analysis of steel cable-stayed bridge." *Structural Engineering and Mechanics*, 11(1), pp. 35-48.

Wang, P. H., Lin, H. T., and Tang, T. Y. (2002). "Study on nonlinear analysis of a highly redundant cable-stayed bridges." *Computers & Structures*, 80, pp. 165-182.

Wang, P. H., Tseng, T. C., and Yang, C. G. (1993). "Initial shape of cable stayed bridge." *Computers & Structures*, 47(1), pp. 111-123.

Wang, P. H. and Yang, C. G. (1993). "Parametric studies on cable stayed bridges." *Computers & Structures*, 60(2), pp. 243-260.

Xi, Y. and Kuang, J. S. (1999). "Ultimate load capacity of cable-stayed bridges." *Journal of Bridge Engineering*, ASCE, 4(10), pp. 14-22.

Yang, Y. B. and Kuo, S. R. (1994) *Theory and analysis of nonlinear framed structures*. Prentice-Hall, Inc., Singapore.